Lithological control on the geomorphic evolution of the Shillong Plateau in Northeast India

Lithological control on the geomorphic evolution of the Shillong Plateau in Northeast India.

Callum M. Strong[1], Mikaël Attal[1], Simon M. Mudd[1], Hugh D. Sinclair[1]

[1]University of Edinburgh, School of GeoSciences, Drummond Street, EH8 9XP, UK

Correspondence to: Callum Strong (C.M.M.Strong@sms.ed.ac.uk)

Abstract

The Shillong Plateau in Northeast India is a block of raised topography in the Himalayan foreland which consists of crystalline basement rocks partially covered by a Cretaceous to Miocene sedimentary succession. It is dominated by a mature, low relief landscape surrounded by high relief, fluvially dissected margins, particularly along its southern flank which is bounded by the Dauki thrust Fault. We use river profiles and geological relationships to show that the low relief plateau is a topographic expression of a re-exposed basement palaeosurface following the stripping of sedimentary cover by scarp retreat. We show that initiation of the wave of incision does not require surface rupture on the Dauki Fault or an increase in fault slip rate at the end of the Miocene, as suggested by previous studies. We propose that incision has been spatially controlled by the slope of the basement palaeosurface, likely moderated by an incision threshold. River profiles in the Shillong Plateau cannot be interpreted as simple records of surface uplift. The observed heterogeneous spatial pattern of steepness is a function of a dynamic landscape response to the erosion of layered lithology with contrasting erodibility. Such dynamics have

implications for fluvial geomorphology, highlighting that near-horizontal lithological contacts can strongly influence river profiles and topography, even when no longer physically preserved. The topography of the northern Shillong Plateau is controlled by the structure of basement rocks and is reminiscent of stable cratonic interior landscapes, consistent with its surface exposure during late Cretaceous times.

Keywords: Shillong Plateau; erosion; lithology; river profile.

1. Introduction

The Shillong Plateau, situated in the Eastern Himalayan foreland in Northeast India, is a regionally important structure reflecting a change in the dynamics of the India – Eurasia collision at the front of the Himalaya (Johnson and Alam, 1991; Grujic et al., 2006; Biswas et al., 2007; Banerjee et al., 2008; Bookhagen and Burbank, 2010; Vernant et al., 2014; Kumar et al., 2015; Najman et al., 2016). The plateau is surrounded to the north, east and south by the Eastern Himalaya, the Indo-Burman ranges and the Bengal basin, respectively (Fig. 1, 2). It influences sedimentation in the Brahmaputra valley and Bengal basin (Najman et al., 2016; Govin et al., 2018), monsoon precipitation in the Himalaya (Grujic et al., 2006; Biswas et al., 2007; Bookhagen and Burbank, 2010) and regional earthquake hazard (Sukhija et al., 1999). The plateau consists of an actively uplifting block of Indian crystalline basement rocks with patchy Cretaceous and Tertiary cover sediments in the west, south and east (Fig. 1, 2). Recognition of the Shillong Plateau's unusual structural setting (e.g., Bilham and England, 2001) has led to intensification of studies in the last decade. Recent evidence from thermochronology (Biswas et al., 2007; Clark and Bilham, 2008) and sedimentology (Najman et al., 2016; Govin et al., 2018) have been seminal in developing a temporal framework for the geological and geomorphological evolution of the Shillong Plateau, in particular for revealing an apparent lag time between rock exhumation (beginning in the Miocene) and surface uplift of the plateau. However, the exact timing of events and the factors driving this lag time and the morphological evolution of the plateau are still currently debated.

Plateau formation and the planation of bedrock surfaces was a subject at the core of 'classical' geomorphology (see reviews by Twidale, 1992; Orme, 2007). In a modern era of

process study and quantification, the focus of geomorphology has largely shifted from ancient Gondwanan landscapes to the study of tectonically active, eroding mountain ranges. The Shillong Plateau exhibits a mix of characteristic features from both tectonically active settings and ancient cratonic landscapes (Migoń and Prokop, 2013; Prokop, 2014). Active, crustal scale thrust faults (Bilham and England, 2001; Mitra et al., 2005) and high relief, fluvially dissected plateau margins are juxtaposed against a relatively low-relief plateau interior complete with mature multi-concave topography and the deep weathering of crystalline basement rocks (Migoń and Prokop, 2013; Prokop, 2014). Based on understanding from many active mountain ranges, it is reasonable to suggest that the erosion of several kilometres of rock in response to sustained rock uplift should result in the development of incised, high-relief mountainous topography. However, despite the erosion of >3 km of sedimentary rocks from the Shillong Plateau since Miocene times (Biswas et al., 2007; Clark and Bilham, 2008), the plateau's topography is distinctly flat. In addition, despite extremely high precipitation rates that can exceed six meters per year (Bookhagen and Burbank, 2006; Rosenkranz et al., 2018), erosion rates are low, between ~0.05 and 0.2 mm/yr, and do not correlate well with precipitation (despite a 7x variation in annual precipitation rates) or landscape steepness (Rosenkranz et al., 2018).

As mentioned above, some studies have highlighted a lag time between the onset of rock uplift and surface uplift of the plateau, which may explain some of the plateau's peculiar geomorphological features. Biswas et al. (2007) and Clark and Bilham (2008) dated the initiation of rock uplift and exhumation to before 8-15 Ma using apatite (U-Th-[Sm])/He and apatite fission track thermochronology. Thermal modelling by Biswas et al. (2007) yielded exhumation rates ranging between 0.2 and 0.6 mm/yr with a later stage deceleration: their

77 samples may have reached the surface ‘as early as, or any time after 5.5-3.5 Ma’. These
78 authors also showed that the sedimentary cover of the northeastern plateau region was
79 minimal relative to the south where a thickness of 3 - 6 km of Upper Cretaceous to Miocene
80 succession has been eroded (Fig. 2). Using stratigraphic analysis and flexural modelling of
81 sediments in the Surma Basin situated immediately south of the Shillong Plateau, Najman et
82 al. (2016) deduced that significant surface uplift of the plateau began 3.5-2 Ma ago,
83 confirming the temporal decoupling between the onset of exhumation in Miocene times
84 and the surface uplift. Rosenkranz et al. (2018) estimated that surface uplift began 3-5 Ma
85 ago by combining catchment-averaged and bedrock erosion rates derived from cosmogenic
86 nuclides concentrations with estimates of volumes eroded inferred from reconstructed
87 palaeosurfaces across the plateau. Finally, Govin et al. (2018) dated the diversion of the
88 Brahmaputra River as a result of the rise of the Shillong Plateau to between 4.9 and 5.2 Ma
89 using detrital zircon U-Pb data, earlier than previous studies. They argue their approach
90 dates initiation of the surface uplift of the Shillong Plateau more sensitively than previous
91 approaches, as only limited topographic uplift is needed before river diversion occurs (unlike
92 flexural loading; Najman et al., 2016).
93
94 To explain the ~4-12 Ma time lag between the onset of exhumation and significant surface
95 uplift, Biswas et al. (2007) proposed a model where the erosional removal of the highly
96 erodible sedimentary cover initially occurred at a rate matching the uplift rate, possibly
97 facilitated by fluvial bevelling by the Brahmaputra, therefore limiting surface uplift (Bufe et
98 al., 2016; Rosenkranz et al., 2018). The authors suggest that when the more resistant
99 crystalline basement rocks were exposed at the surface, erosion could no longer keep pace
100 with rock uplift and significant surface uplift began. This model, which accounts for the late

stage deceleration evidenced in the thermochronology studies (Biswas et al., 2007; Clark and Bilham, 2008), has since been supported by erosion rates derived from detrital cosmogenic nuclide concentrations in bedrock and river sands, combined with topographic analysis (Rosenkranz et al., 2018).

In a challenge to the Biswas et al.'s (2007) model of exhumation / uplift decoupling, Govin et al. (2018) argue that the ~3.5 Ma lag between the deflection of the Brahmaputra River (supposedly resulting from initiation of the surface uplift) and the arrival of significant amounts of basement-derived sediment from the Shillong Plateau in the Surma Basin (after 1.5 Ma, as presented in Bracciali et al., 2016, and Najman et al., 2012) is evidence that the exhumation of more resistant basement rock 'is not the dominant factor responsible for the change from exhumation to surface uplift'. The authors argue for an increase in the Dauki fault slip rate, which would be consistent with the substantial increase in the rotation of the Shillong block in the past 4-8 Ma needed to explain the discrepancy between GPS-measured convergence rates and long-term uplift rates across the region (Vernant et al., 2014). The findings of key studies regarding the chronology of Shillong Plateau uplift are summarised in Table 1.

Building on the numerous studies which have used topographic data as ancillary support for various geological models of the Shillong Plateau's evolution (e.g., Bilham and England, 2001; Rajendran et al., 2004; Biswas et al., 2007; Clark and Bilham, 2008; England and Bilham, 2015; Najman et al., 2016; Rosenkranz et al., 2018), we combine topographic analysis of river channels, field observations and recent numerical model developments to re-evaluate the controls on the Shillong Plateau's topographic and erosional patterns. In particular, we

ask whether the Biswas et al.'s (2007) model of topographic evolution featuring the differential erosion of rocks with contrasting resistance to erosion can be invoked to account for the existing discrepancies between (i) the thermochronological and morphological records of surface uplift and (ii) the arrival of significant amounts of basement-derived sediment in the sedimentary basin to the south. We also investigate whether the topography of the Shillong Plateau can be used to infer information about its large scale tectonic structure, notably the location and character of major plateau bounding faults.

2. Study Area

The Shillong Plateau is an approximately rectangular (elongated east to west) area of topography at an average elevation of ~1200 m (maximum >2000 m) covering ~ 30000 km^2 (Fig. 1). Numerous studies have noted the prominent headward erosion signals propagating through the rivers draining the southern plateau margin, evidenced by large-scale knickzones in the channel network (e.g., Biswas et al., 2007; Prokop, 2014; Rosenkranz et al., 2018) (Fig. 1). While some knickpoints are associated with lithological boundaries at the local scale (Migoń and Prokop, 2013; Prokop, 2014), many major knickpoints in south-draining catchments do not correlate with lithological contacts, instead suggesting this signal is associated with the propagation of an erosional front in response to tectonic uplift (e.g., Biswas et al., 2007; Rosenkranz et al., 2018) (Fig. 1). The high relief of the southern plateau margin orographically focusses extreme Indian Summer Monsoon precipitation and makes it officially the wettest place in the world; annual precipitation can exceed a record breaking 26000 mm and single day rainfall totals of >1500 mm have been recorded (Murata et al., 2007). There is a strong orographic precipitation gradient increasing north to south

149 across the Shillong Plateau, with annual precipitation varying from 1600 mm in the
150 Brahmaputra valley to the north to 6000-12000 mm on the southern edge of the plateau
151 (Murata et al., 2007; Prokop, 2014).
152
153 Estimates of the India – Eurasia crustal shortening accommodated across the Shillong
154 Plateau vary from 0.7-2.3 mm/yr (Biswas et al., 2007) to 4-7 mm/yr (Banerjee et al., 2008).
155 This shortening is accommodated by plateau bounding, crustal scale faults to the north and
156 south (Bilham and England, 2001), although the detailed structure remains contentious (e.g.,
157 Najman et al., 2016). The Dauki Fault follows the linear southern plateau margin and is
158 recognised as a steep north-dipping thrust fault (Fig. 1) that is primarily responsible for
159 plateau uplift (Bilham and England, 2001); whether the strikingly linear southern boundary
160 of the plateau actually represents the Dauki fault trace at the surface or the axial trace of a
161 large scale, south-vergent monocline produced by a Dauki Fault that only exists at depth, is
162 debated (Clark and Bilham, 2008).
163
164 Following modern analysis of observations originally made by Oldham (1899) from the
165 'Great Assam Earthquake' in 1897 (M_w = ~8.3), Bilham and England (2001) proposed the
166 existence of a steep, south-dipping, ~NW-SE trending thrust fault at depth in the north of
167 the plateau, which has been interpreted as the structural boundary of the plateau to the
168 north. Despite the strength of geological and seismic evidence for the 'Oldham Fault'
169 (Bilham and England, 2001; Biswas et al., 2007; Kayal et al., 2012; England and Bilham, 2015),
170 as well as evidence from a series of geomorphic indices (e.g., slope-area analysis by Clark
171 and Bilham, 2008; valley depth by England and Bilham, 2015), the contrast in the
172 topographic expression of faults between the south and the north of the plateau led some

authors to question the importance of the Oldham Fault within the modern tectonic framework (Rajendran et al., 2004). The topographies of the western and south-eastern regions of the Shillong Plateau are influenced by different tectonic regimes: to the west, the Dauki fault becomes less important and another major tectonic feature, the Dapsi Thrust, dominates (Fig. 2); in the southeast, the Dauki fault undergoes a complex transitional interaction with the Haflong-Disang Faults and the Indo-Burman ranges (Fig. 2). As such, this study is limited to consideration of the central Shillong Plateau to the north of the Dauki Fault, where the findings of recent thermochronology and tectonic studies enable integration with the geomorphology.

3. Methods

Our study is based on the analysis of topographic data and direct field observations. We use 30-m resolution Digital Elevation Models (DEM) from the Shuttle Radar Topography Mission (SRTM) which can be downloaded freely from the Open Topography website: http://www.opentopography.org/. To link changes in morphology to potential changes in rock types exposed or to the presence of faults, geological maps from Yin et al. (2010) and Mukherjee et al. (2012a, 2012b, 2013a, 2013 b, 2013c, 2014) were georeferenced using the spatial references provided within; where spatial references generated poor correlation with the observed topography within the geographic projection used (World Geodetic System (WGS) 1984, Zone 46N) or were absent, georeferencing was performed using distinctive topographic features expressed in the geological maps. The morphology of the plateau was analysed as a whole through comparison of topographic and swath profiles, whereas rivers were analysed through their profiles and plan view using an approach that

integrates drainage area along flow length (the so-called 'integral approach', e.g., Perron and Royden, 2013), as described below.

In unglaciated, eroding landscapes, fluvial incision sets the base level for all other geomorphic erosion processes. To investigate landscape evolution, it is therefore appropriate to examine spatial patterns of erosion in rivers (e.g., Stock and Montgomery, 1999; Kirby and Whipple, 2001; Kirby et al., 2003; Snyder et al., 2003; Wobus et al., 2006; Miller et al., 2007; DiBiase et al., 2010; Kirby and Whipple, 2012). For over a century, workers have reasoned that steeper channel slopes should result in faster erosion, all else equal (e.g., Gilbert, 1877). However, casual observers of topography have noted that headwaters are steeper than lowland channels, leading many authors to propose that erosion should also correlate with discharge (e.g., Howard and Kerby, 1983). A normalization is therefore required to compare channel gradients for channels of different discharge (or drainage area, often used as a proxy for discharge). Morisawa (1962) and Flint (1974) noted that a number of properties of channels, such as gradient (*S*) and drainage area (*A*), are related via power laws, and proposed the following relationship:

$$S = k_s A^{-\theta} \quad (1).$$

The two empirical coefficients, k_s and θ, are called the steepness index and concavity index respectively, as k_s defines how steep the slope *S* of a river is for a given drainage area *A*, and θ defines how concave a river profile is by controlling how quickly slope increases when drainage area decreases. Many authors have found a relationship between measured erosion rates and k_s (Ouimet et al., 2009; DiBiase et al., 2010; Scherler et al., 2014; Mandal

et al., 2015; Harel et al., 2016). Spatial variations in the steepness index have therefore frequently been interpreted in terms of spatial variations in erosion or rock uplift rates assuming homogenous erodibility of the bedrock (e.g., Kirby and Whipple, 2012). However, the gradient S needed to calculate k_s suffers from a substantial amount of noise when derived from topographic data (e.g., Wobus et al., 2006). To avoid this problem, Royden et al. (2000) suggested integrating drainage area along flow distance to create normalized river profiles as a function of elevation. Because the slope term in equation (1) is the same as the derivative of elevation with respect to distance (i.e., $S = dz/dx$), equation (1) may be integrated from an arbitrary base level location (x_b) to any point along the channel, x (e.g., Whipple et al., 2017a):

$$z(x) = \mathrm{z}(x_b) + \left(\frac{k_s}{{A_0}^{-\theta}}\right) \int_{x_b}^{x} \left(\frac{A_0}{\mathrm{A(x)}}\right)^{\theta} dx \quad (2),$$

where A_0 is a reference drainage area, introduced to nondimensionalize the integrand in equation (2). We can then define a longitudinal coordinate, χ, with dimensions of length (Royden et al., 2000; Perron and Royden, 2013):

$$\chi = \int_{x_b}^{x} \left(\frac{A_0}{\mathrm{A(x)}}\right)^{\theta} dx. \quad (3).$$

The longitudinal coordinate χ ('chi') is defined in such a way that:

$$z(x) = \mathrm{z}(x_b) + \left(\frac{k_s}{{A_0}^{-\theta}}\right) \chi \quad (4).$$

The coordinate can be calculated from topographic data for a fixed 'reference' value of θ (called θ_{ref}). If we set A_0 = 1 m^2, then from equation (4) we see that the 'normalized' steepness index (i.e., steepness index for a fixed value of θ, called k_{sn}) is the local slope of the elevation profile in χ-space. Using these transformed river profiles, we can compute the normalized steepness index and make inferences about the causes of spatially varying k_{sn}, including variations in erosion rates and/or bedrock erodibility.

Accordingly, longitudinal river profiles from 15 major catchments (Fig. 3) radially draining the Shillong Plateau were extracted from the 30-m resolution SRTM data. All χ coordinates for production of k_{sn} maps and χ profiles were calculated using a reference θ_{ref} of 0.5, which was determined as the best fit for the study area following the methods of Mudd et al. (2018); this value is in the range of expected concavity values (typically $0.35 \leq \theta \leq 0.65$, e.g., Hack, 1957; Wobus et al., 2006; Kirby and Whipple, 2012). Longitudinal and χ profiles were produced for all main channels and all connecting tributaries, and k_{sn} values were extracted using the method of Mudd et al. (2014).

Where drainage basins share a base level, map visualization of the longitudinal χ coordinate can reveal disequilibrium (or lack of it) between competing drainage basins (Willett et al., 2014; Giachetta et al., 2014). High contrasts in χ coordinate across a drainage boundary may indicate that the basin with lower χ values aggressively gains area via river capture and divide migration at the expense of the neighboring catchment (Willett et al., 2014). Recent work has questioned the reliability of this method to assess the competition between large basins with spatially distant base levels, as local changes in uplift rate or rock type can influence the χ coordinate (Whipple et al., 2017b). However, we believe the method can

highlight relatively recent drainage reorganizations along divides shared by catchments with outlets in close proximity, such as adjacent tributaries. Therefore, we produced a map of the χ coordinate to investigate equilibrium between major catchments draining either to the south or to the North of the Shillong Plateau, in order to shed light on the evolution of catchment shape. We anticipate seeing a correlation between high χ contrasts across drainage divides and evident river capture events. River captures can also be identified by visual identification of headless channels in Google Earth satellite imagery. The southern catchments for which we plot χ coordinates all drain to the Bangladeshi plain along the Surma River, all having an outlet elevation of 10-15 m which we assume corresponds to a common base level. For the northern catchments, we used the Brahmaputra River as the common base level (elevation of 40-55 m).

4. Results

4.1. Elevation, relief and drainage network planform.

The southern and central plateau is characterized by a high elevation (1000-2000 m) relatively low relief (50-150 m) plateau surface forming a large scale topographic dome with typical surface slopes of 0-5° (Fig. 1, 4), dipping most steeply in a southerly direction towards the Dauki fault. At the local scale, this surface is characterized by convex rolling hills with alluvial river valleys. Along the southern plateau margin and in the northwest of the plateau, this low relief surface has been spectacularly incised by rivers, resulting in up to 1500 m of vertical relief (Fig. 1, 4, 5). Valley depth along the southern margin is greatest in the center of the Plateau and decreases towards the east and west (Fig. 4).

The landscape in the northeast of the Plateau has a lower elevation (500-1000 m) and features more uniform relief; the sharp topographic contrast between incised valleys and plateau surfaces observed in the southern plateau is absent (Fig. 4). The boundary between the northern plateau margin and the Brahmaputra valley sedimentary basin is highly irregular, appearing topographically 'filled' by valley sediments (with valley sediment onlapping on steep valley sides; Fig. 1). This contrasts with the linear boundary of the southern plateau (Fig. 1), which has been suggested to represent the linear trace of the Dauki Fault (Biswas and Grasemann, 2005).

As mentioned in the methods section, the difference in base level elevation between northern and southern catchments, as well as the morphological complexity of the ~500 km-long stretch of the Brahmaputra River between where northern and southern catchments join, preclude a direct comparison of χ values between northern and southern catchments. However, longitudinal χ coordinate mapping can be used to reveal potential (dis)equilibrium between catchments sharing the same base level (northern catchments and southern catchments). Southern catchments that drain across the Dauki Fault show significant differences in χ values across internal drainage divides, particularly around the northern edges of interfluve plateau remnants surrounded by deeply incised river valleys (Fig. 6). This difference in χ values across internal drainage divides suggests ongoing drainage reorganization (e.g., Willett et al., 2014). Abundant headless channels, indicative of river capture, are evident on these plateau remnants and preferentially occur where plateau remnants are bound to the north by deeply incised channels (Fig. 6). Differences in χ coordinate are also notable along the divide separating the Umngot catchment (#14) from the Myntdu catchment (#15) to the east (Fig. 3, 7a). Differences in χ coordinate between

314 northern catchments are not as prominent, except in the narrowest stretch of the Umiam
315 catchment (#6). Catchments in the southwest of the Shillong Plateau all display some
316 preferential elongation in the northeast to southwest direction. Similarly, many catchments
317 draining to the northeast of the plateau are also elongated in the NE-SW direction,
318 demonstrated to an extreme degree by the Umiam catchment (#6, Fig. 3).
319
320 ## 4.2. Spatial patterns of channel steepness
321 Before interpretation of channel elevation and χ profiles, it is important to identify spatial
322 changes in lithology which would influence rock erodibility and therefore channel steepness.
323 The task of determining exactly where lithological contacts are in the Shillong Plateau is
324 complicated by significant spatial disagreements between the primary sources used (e.g.,
325 Yin et al., 2010; Mukherjee et al., 2012a, 2012b, 2013a, 2013b, 2013c, 2014). Lithological
326 contacts in Yin et al. (2010) often follow topographic features and lineaments, suggesting
327 that some contacts were surveyed using satellite imagery. When disagreement occurs, we
328 refer to the Geological Survey of India's District Resource Map series by Mukherjee et al.,
329 (2012a, 2012b, 2013a, 2013b, 2013c, 2014) which is based on field mapping. Linear
330 geological features are exploited by rivers throughout the plateau (Gupta and Sen, 1988;
331 Das et al., 1995; Biswas and Grasemann, 2005; Yin et al., 2010; Duarah and Phukan, 2011)
332 and evidence heterogeneities in lithological erodibility. However, while significant plan-form
333 control on flow routing is exerted by these features, comparison of linear channels with
334 their non-linear neighbours reveals limited elevation differences in the south and central
335 plateau region, suggesting that the extent of perturbations in long profile form driven by
336 these linear features is limited in the context of the large vertical scales (> hundreds of
337 meters) considered in this analysis. However, the preferential exploitation of linear features

by river channels appears to significantly perturb channel profiles in the north-eastern plateau region.

In a framework where fluvial incision rates scale with stream power or shear stress, river profiles are expected to be inherently sensitive to long-term changes in precipitation. Records from cave speleothems (Berkelhammer et al., 2012, Dutt et al., 2015) suggest that monsoon strength fluctuates cyclically on millennial timescales, but records from ocean sediments (Dettman et al., 2001) reveal that strong Indian Summer Monsoons have been persistent for over 10 Ma. As the exhumation history of the plateau falls largely within this timeframe, we assume channel profiles in the Shillong Plateau have not been significantly perturbed by long-term climatic variability.

If we assume k_{sn} values can be used as a proxy for erosion rates (e.g., Kirby and Whipple, 2012), the k_{sn} data suggest that all southern catchments are experiencing high erosion rates in the 30-50 km upstream of the Dauki Fault (Fig. 7b, 8). This however is inconsistent with the low erosion rates derived from ^{10}Be concentrations in river sands for these steep, deeply incised channels, broadly on the order of 0.05 – 0.1 mm/yr (Rosenkranz et al., 2018). Therefore any interpretation of channel morphology must take into account the apparent discordance between the steep, incised topography along the southern boundary of the plateau and the low erosion rates inferred from ^{10}Be concentrations. These 'incised channels' are almost exclusively eroding basement rocks (Fig. 9) and changes in slope along the river profiles were found to not always coincide with recorded changes in lithology within the basement units (see also Prokop, 2014).

362 The upper reaches of south draining channel networks typically display much lower k_{sn}
363 values, consistent with the low relief landscape we observe in the central plateau (Fig. 7b, 8).
364 Some minor knickpoints are evident in these channel segments and many correlate with
365 lithological variations, e.g., remnant patches of sediments where the sedimentary bedding is
366 expressed in the elevation profiles as noted by Prokop (2014). Henceforth, these low k_{sn}
367 channels are referred to as 'plateau-top channels'. The plateau-top channels are parallel in χ
368 plots, suggesting spatially homogenous, low erosion rates (Fig. 8). This result is consistent
369 the independent records of exhumation from thermochronology which show that the
370 modern plateau surface must have been buried under a minimum of 3 km of sediment but
371 that exhumation has been extremely slow over the last 5.5-3.5 Ma (Biswas et al., 2007; Clark
372 and Bilham, 2008). It is also supported by recent ^{10}Be data showing extremely low bedrock
373 erosion rates on the plateau surface, ranging between 0.002 and 0.006 mm/yr (Rosenkranz
374 et al., 2018). Catchment-averaged erosion rates from ^{10}Be concentrations in river sand on
375 the plateau surface were found to be surprisingly very high, higher than in the incised
376 channels, on the order of 0.14 – 0.2 mm/yr (Rosenkranz et al., 2018); however, the authors
377 attribute the high rates to recent anthropogenic disturbance (deforestation and soil
378 degradation).
379
380 Geological maps and cross-sections show that the plateau surface approximates the
381 exposed contact between the sedimentary cover and the crystalline basement (Biswas et al.,
382 2007). This is evidenced by the preservation of small patches of Palaeogene and Cretaceous
383 marine sediments scattered across the central plateau and found >50 km north of the
384 southern plateau margin, appearing as thin veneers on cross-sections (Mukherjee et al.,
385 2012a, 2012b, 2013a, 2013b, 2013c, 2014) (Fig. 10). This outcrop pattern shows there has

been almost complete erosion of the sedimentary cover rocks but only limited incision into the basement rocks of the central plateau. The surface created by the stripping of this stratigraphic contact is evident in topographic profiles (Fig. 4) and accounts for the systematic variations in the elevation of plateau-top channel segments observed in χ plots (i.e., dome shape reflected in decreasing plateau-top channel elevation east and westwards, away from the centre, Fig. 8). These observations suggest that the long profile morphology of the plateau-top channels is controlled by a low-relief palaeosurface that forms the stratigraphic contact between the sedimentary cover and the basement rocks. The low slope of this exposed palaeaosurface limits the erosive potential of these channels, consistent with the low values of k_{sn} observed. It is important to note that, in places, the high contrast in erodibility is found within the sedimentary cover, as the lowest sedimentary unit can be more resistant to erosion than the overlying sedimentary layers (Fig. 5b). In most places, the boundary between erodible and resistant rocks is found at, or within 200 m of, the sediment-basement contact.

Convex-up channels incising uniform lithology upstream of an active fault are typically interpreted as recording an increase in the displacement rate on the fault (e.g., Whittaker et al., 2008; Attal et al., 2011; Kirby and Whipple, 2012). In a χ-plot, such channels would appear with an inflexion point separating a steep section upstream of the fault (section adjusted to the new throw rate) and a less steep section upstream of the inflexion point representing the 'relict' landscape that has not yet responded to the change in throw rate. The gradient of the χ-profile represents the channel steepness k_{sn} (Royden et al., 2000; Perron and Royden, 2013). Within a given catchment, channels and tributaries incising uniform lithology are expected to collapse into a single profile in χ–elevation space; if

adjacent catchments are experiencing similar forcing, they too are expected to collapse on the same profile. Whereas the χ-plots of the southern catchments display such form overall, we note spatial variations in k_{sn} between and within these catchments that are inconsistent with this model (Fig. 7b, 8). While some noise is expected in real channel networks, χ-plots of southern draining rivers reveal channel networks where different channels display markedly different gradients in χ-elevation space (Fig. 8: see for example catchment 14 - the Umngot River). Plateau-top channels systematically plot at different elevations with similar gradients in χ-elevation space, tracing the stratigraphic contact between basement rocks and cover sediments.

Channel networks with outlets on the northern margin of the plateau (Fig. 11) display patterns of steepness similar to those observed within the southern channel networks, with low-gradient plateau-top channels connecting to the Brahmaputra River via steep channels; the vertical magnitude of the knickzones (steepened reaches) is variable, from 400 to in excess of 1000 m (Fig. 11). In general, the northern catchments are more heterogeneous than the southern catchments, with significant within-catchment variability in channel steepness. As they reach the Brahmaputra valley, some of the northern channels undergo a dramatic downstream transition from a continuously steep bedrock channel dominated by large boulders to a low gradient, sandy alluvial channel; the change can occur very abruptly (e.g., within ~100 m on the Umkhen River #7, Fig. 3, 11; see transition at latitude 25.957204 and longitude 92.519296 on Google Maps, retrieved 18/07/2018) and is not coincident with an obvious change in valley relief. The main topographic differences with the southern margin are that the plateau margin is irregular in plan-form (instead of linear) and that the dissection is more irregular than and not as dramatic as in the south.

4.3. Scarps as significant morphological features on the plateau

A number of topographic scarps exist on the Shillong Plateau. Notably, the 50 km long, ~500 m high, northeast facing Khri scarp in the center-north of the Shillong Plateau, delineates the most northerly extent of the high-altitude, low relief plateau landscape (Fig. 1). Channels that dissect this scarp display high k_{sn} values upstream (Fig. 1, 7, 10). The Khri scarp is cut into basement rocks and does not correlate with any lithological contacts in geological maps (Mukherjee et al., 2012a, 2012b, 2013a, 2013b, 2013c, 2014). Another 30 km long, 400 m high, northeast facing scarp, is located at the southwest corner of the plateau, following the SW side of the Kynshi River (river #9, Fig. 1, 3).

The Kynshi scarp is made of Cretaceous – Paleogene cover sediment and its base coincides with the contact with the crystalline basement rocks. Similar, although smaller and less extensive, north-facing scarps, are present in the sedimentary rocks perched on the interfluvial plateau remnants along the southern plateau margin (Fig. 1). Similar to the Kynshi scarp, the base of these scarps is controlled by planar stratigraphic contacts between the sedimentary cover and either basement rocks or the oldest, hardest sedimentary strata immediately on top of the basement.

5. Discussion

5.1. Drainage network planform and river capture

Despite not being able to compare χ values across the divide separating northern and southern catchments (due to differences in base level), longitudinal χ coordinate mapping

457 reveals overall equilibrium between major catchments, demonstrating the planform
458 stability of the large-scale drainage network in the Shillong Plateau. At the local scale,
459 significant differences in χ coordinates across drainage divides do occur. Across-divide
460 differences in the Umiam catchment (#6) may reflect the natural propensity for an
461 extremely narrow catchment to widen, whereas the differences along the eastern boundary
462 of the Umngot catchment (#14) (Fig. 3, 7a) may indicate progressive plateau integration and
463 drainage area gain, consistent with the observation that the eastern branch of the Umngot
464 is more entrenched than its neighbours on the plateau (Fig. 1, 3). Differences in χ values
465 and abundant headless channels observed in south draining catchments show internal
466 drainage reorganisation; river capture is actively occurring around the northern edges of
467 interfluve plateau remnants surrounded by deeply incised river valleys. The depth of incision
468 of the captor channel is typically more than one order of magnitude greater than that of the
469 headless, victimized channel: the low entrenchment of plateau top-channels (low relief) is
470 likely to facilitate capture by their deeply incised neighbours.
471
472 The general trend for the NE-SW elongation of catchments on the Shillong Plateau is
473 directionally coincident with the dominant structural fabric of the sheared basement rocks
474 and the trend of the Badapani-Tyrsad shear zone (Fig. 1). Yin et al. (2010) argue for Tertiary
475 activity of the Badapani-Tyrsad shear zone based on its notable topographic expression, the
476 spectacular elongation of the Umiam catchment (#6, Fig. 3) and hair-pin geometry of the
477 same river observed crossing the fault. However, examination of the numerous sections of
478 rivers crossing the proposed shear zone and, presumably, experiencing the same proposed
479 offset reveals only a single example of such geometry. Additionally, the magnitude of lateral
480 offset required to shear catchments to the observed degree is not realistic in the wider

481 geological context of the plateau: catchment width is more than an order of magnitude
482 shorter than catchment length, which would require tens of km of displacement (see Hallet
483 and Molnar, 2001).
484
485 Where catchments are being actively sheared, dynamic reorganisation of drainage basins is
486 to be expected, which should lead to systematic differences in χ values at divides (Hallet and
487 Molnar, 2001; Castelltort et al., 2012; Goren et al., 2015). However the overall inter-
488 catchment equilibrium revealed by the χ coordinate map of the Shillong Plateau (Fig. 7a)
489 suggests active shearing of catchments is unlikely to be occurring. Instead, we attribute
490 catchment elongation to differential erosion of previously sheared basement rocks, creating
491 NE-SW trending topographic ridges which serve to isolate catchments, and linear
492 weaknesses that entrain rivers. Indeed, lineaments topographically expressed by
493 preferential river incision are common throughout the Shillong Plateau (Fig. 1). These
494 features have been noted by a number of authors who have attempted to use satellite
495 imagery to map the structure of the basement rocks and infer tectonic information (e.g.,
496 Gupta and Sen, 1988; Das et al., 1995; Biswas and Grasemann, 2005; Yin et al., 2010; Duarah
497 and Phukan, 2011).
498
499 ## 5.2. Topographic evolution of the northern Shillong Plateau
500 The northern plateau margin with the Brahmaputra valley sediments is convoluted,
501 suggesting that it is not directly fault-controlled. The intricate plateau margin and outcrops
502 of basement rocks north of the Brahmaputra, observed to within 30 km of the Himalayan
503 mountain front (Fig. 2), imply that the basement surface underneath the alluvial sediments
504 of the Brahmaputra valley is highly irregular. The abrupt transition from steep boulder and

505 bedrock channels to alluvial channels along the boundary of the plateau (e.g Umkhen River,
506 see section 4.2), combined with no obvious change in valley relief at this transition, and the
507 very low relief across the Brahamputra valley, imply recent aggradation leading to the burial
508 of pre-existing topography.
509
510 Thermochronology data show the basement rocks of the northern Plateau region were
511 exposed in the late Cretaceous, buried under 1.15 to 2.75 km of sediment, and exhumed in
512 the late tertiary (Biswas et al., 2007). This implies that rock uplift led to the entire stripping
513 of this post-Cretaceous sedimentary package and exposure of the basement rocks along the
514 northern margin of the plateau. The knickzones along the northern channels may represent
515 the topographic response to uplift and local steepening driven by faulting of crustal flexure
516 (e.g., Clark and Bilham, 2008), or may be antecedent landscape features that were buried
517 during the late Cretaceous – Tertiary and re-exhumed following the post-Miocene uplift of
518 the plateau.
519
520 We hypothesise that the base-level fall signal needed to expose the basement along the
521 northern channels (Fig. 11) is punctuated by 'noisy' dynamic fluctuations in the elevation of
522 Brahmaputra valley sediments, consistent with the observation by Rajendran et al. (2004) of
523 abundant patches of "older alluvium" fringing basement rock outcrops in the Brahmaputra
524 valley. Such scenario seems reasonable, as the Brahmaputra has the highest sediment load
525 of all the rivers on Earth (Milliman and Syvitski, 1992) and sediment pulses can be generated
526 by stochastic events such as earthquakes (e.g., Schwanghart et al., 2016) and floods (Sarma,
527 2005). In short, channel morphology in the northern region is complex and possibly
528 controlled by the inheritance of ancient river channels that were buried under sediment in

529 the late Cretaceous (Biswas et al., 2007). It seems probable that this Cretaceous landscape
530 effectively continues underneath the Brahmaputra valley, buried under Cretaceous –
531 Tertiary cover (Clark and Bilham, 2008) that is itself covered in modern alluvium. High-
532 resolution imaging of the basement surface underneath the Brahmaputra valley sediments
533 could test the interpretations presented here and provide key insights into the evolution of
534 the northern plateau.
535
536 ## 5.3. Stripping mechanisms in the southern Shillong Plateau
537 Topographic and geological observations reveal the almost complete stripping of the
538 sedimentary rocks that cover basement units across the southern and central plateau region,
539 re-exposing a basement palaeosurface which forms the modern plateau surface (Fig. 4, 10).
540 As the landscape has inherited the topography of this exhumed, low-gradient, low-relief
541 palaeosurface, it has also inherited low slopes which limit the rate of erosion in channels
542 and on hillslopes and encourages the development of an apparently mature landscape (Fig
543 5a). The shape of the basement palaeosurface has been slightly modified by deformation
544 from a once presumably flat landscape, as evidenced by its domed shape (e.g., Fig. 4),
545 leading to spatial variation in plateau surface slopes (Rosenkranz et al., 2018).
546
547 The observation of large, abundant scarps in the remnants of sedimentary cover suggests
548 that scarp retreat may have been an important process in generating the modern
549 topography of the Shillong Plateau. Indeed, scarp retreat has been identified as a
550 fundamental process of landscape evolution in many landscapes where significant
551 thicknesses of sub horizontal, well-stratified sediments are being eroded, for example: in
552 the Colorado Plateau in the southwest USA (e.g., Schmidt, 1989); in the Chapada do Araripe

plateau in Northern Brazil (de Carvalho Júnior, 2015; Peulvast and Bétard, 2015); in the Tepui landscape of the Gran Sabana in Venezuela (Piccini and Mecchia, 2009; Mecchia et al., 2014). Karstic cave formation and subsequent collapse has been shown to be an important mechanism for generating the scarp-bound Tepui plateaus in Venezuela (Wray, 2009; Mecchia et al., 2014). The abundance of caves and karst formations in the sediments of the Shillong Plateau suggests this process may also have played an important role in the plateau's landscape evolution. The scarps observed in remnant sedimentary rocks in the Shillong Plateau (e.g., Kynshi Scarp, Fig. 1) consistently face the center of the plateau, counterintuitively suggesting scarp retreat from the center of the plateau towards the Dauki Fault. This model is consistent with the observation that all the remnant sedimentary cover is found along the edge of the southern plateau margin (Fig. 2, 10). We might intuitively expect the preservation of sedimentary remnants at the highest elevation regions in the central plateau (e.g., Braun et al., 2014), so how can this spatial pattern of sedimentary cover be explained?

Recent theoretical work investigating the evolution of landscapes composed of layered rocks characterized by differences in erodibility provides a possible explanation: Forte et al. (2016) used an evolution of the Channel-Hillslope Integrated Landscape Development (CHILD) model (Tucker et al., 2001) to investigate the erosion of a stratigraphic package of two different lithologies with different erodibilities (one 'hard' and one 'soft'). They modelled a scenario where a landscape with an open boundary on one side ('south') is uplifted at a constant rate; softer rocks overlie hard rocks, with a contact dipping 5° towards the open boundary. This situation is almost directly analogous to the geological setting of the southern Shillong Plateau, where several km of sedimentary rock overlaid presumably

577 less erodible crystalline basement along a planar contact dipping ~5° south towards the
578 Dauki fault, with catchments also draining southwards (Fig. 12). The results from this
579 numerical experiment show uniformly high erosion rates across the entire surface of the
580 softer lithology until the underlying hard lithology is exposed, first at the upstream
581 boundary ('north') (Forte et al., 2016). A wave of low erosion rates then propagates through
582 the landscape from north to south, as more resistant rocks are progressively exposed,
583 eventually leaving only small patches of soft rock perched on high interfluvial ridges near
584 the outlet boundary (south). The exposure of the hard rocks leads to the development of a
585 low relief surface with erosion rates significantly lower than the rock uplift rate, thus driving
586 surface uplift. When most of the softer lithology has been eroded away, a pulse of incision
587 develops in the lower reaches of the channels (south) and begins generating significant
588 relief in the underlying hard rocks. The spatial pattern of erosion rates in the landscape at
589 the stage when only minor remnants of the softer lithology remain near the outlet boundary
590 closely resembles the spatial pattern of steepness that our topographic analysis reveal in
591 the Shillong Plateau. Additionally, the pattern of sedimentary rocks left along the southern
592 plateau margin (Mukherjee et al., 2012a, 2012b, 2013a, 2013b, 2013c, 2014) bears a striking
593 similarity to these model results (Fig. 10). Forte et al. (2016) found that the dynamic
594 patterns of landscape evolution were extremely sensitive to the slope of the stratigraphic
595 contact: with a horizontal contact, soft rock was stripped in the opposite direction, from the
596 open boundary upstream through the channel network. Therefore we suggest, with the
597 benefit of insights from theoretical work (Braun et al., 2014; Forte et al., 2016), that the
598 slope of the contact between the sedimentary cover and the basement rocks (~5° towards
599 the south in the southern plateau) plays a fundamental role in controlling the observed

distribution of remnant sedimentary cover, the direction of scarp retreat and indeed landscape evolution as a whole (Fig. 12).

Further, we seek to explain the observed variability in channel profiles along the southern margin of the plateau. The degree and depth of incision in incised channels appears to positively correlate with the slope of the plateau/basement surface: catchments at the eastern and western extremities, where the plateau surface is more gently sloping, are less deeply incised than in the centre of the southern region: deepest incision correlates with steepest plateau surface slopes (Fig 1, 4a). Thus, the variability in channel profiles and incision depths can hypothetically be accounted for by a model of incision dependent on the slope of the inherited basement contact surface, though we note that slope and total potential relief are correlated due to the dome shape of the palaeosurface (Fig. 4). However, this model does not satisfactorily account for the abruptness of the amphitheatre-like headwalls of the incised channel valleys: if incision depth were directly dependent on plateau surface slope, we would expect gradual diffusion of the incised valleys into the plateau, as the slope of the basement tends to gradually increase away from the centre of the dome.

We therefore speculate the existence of a critical threshold slope and/or sediment flux that must be exceeded to generate significant incision. Once this threshold has been exceeded and incision has begun, it is plausible that incised reaches may experience a positive erosional feedback following the generation of sediment for use as ‘tools’ for erosion (e.g., Gilbert, 1877; Sklar & Dietrich, 1998, 2001, 2004), although knickpoints may struggle to retreat headward if starved of sediment due to slow erosion in the plateau-top channels.

624 Brocard et al. (2016) demonstrated that high-elevation, low-relief relict landscapes can limit
625 the rate of headward incision in steep downstream channels by moderating the flux and
626 grain size distribution of sediment (see also Attal et al., 2015), thereby limiting erosion. A
627 similar model would neatly account for the amphitheatre morphology of the incised river
628 valleys along the southern plateau margin. This model could also explain the surprising
629 preservation of the low-relief plateau landscape in what would initially appear a highly
630 erosive setting: rapid uplift combined with record-breaking precipitation.
631
632 However, this positive erosional feedback is challenged by recent ^{10}Be-derived, low erosion
633 rates in the incised portions of the southern catchments (~0.05 – 0.1 mm/yr), which appear
634 inconsistent with the exceptionally high precipitation rates and very steep channels and
635 hillslopes (Rosenkranz et al., 2018). Rosenkranz et al. (2018) explain this observation by
636 highlighting that low precipitation variability relative to a high erosion threshold in resistant
637 rocks, as well as dense vegetation cover on hillslopes, may inhibit erosion. Our work builds
638 on this hypothesis, in particular regarding the influence of thresholds. We do believe that
639 there is enough precipitation variability to drive significant floods, as evidenced by very clear
640 high-flow lines separating densely vegetated hillslopes from clean, polished bedrock
641 surfaces in all channels; such lines were found up to 20 m above dry season low-flow lines
642 (Fig. 9). However, our widespread observation of steep bedrock reaches strewn with
643 boulders that are several metres in diameter and exhibit extensive potholes and flutes (Fig.
644 9) indicates long-term stability: such large boulders will only be moved during the very
645 highest discharge, or following size reduction through abrasion (e.g. Cook et al., 2018). This
646 observation highlights a potential negative feedback that is initiated once incision has
647 reached a given amount: the formation of deep narrow gorges will lead to increased

delivery of large blocks (via rockfalls and landslides) which may in turn inhibit river incision (Howard et al., 1994; Attal, 2017; Shobe et al., 2018).

5.4. Topography and tectonic models of Shillong Plateau structure

Different authors have favoured different interpretations of the major tectonic structures that drive the uplift and exhumation of the Shillong Plateau. The linear southern boundary of the plateau has variably been interpreted as representing the location of a surface-rupturing Dauki fault (following the "pop-up" model of Bilham and England, 2001) or as the axial trace of a large scale, south-vergent monocline produced by a Dauki Fault that only exists at depth (Clark and Bilham, 2008) (Fig. 12). There is debate about which, if any, major fault(s) control uplift on the northern side of the Shillong Plateau (Rajendran et al, 2004; Yin et al., 2010). Here we discuss the relevance of our topographic and geological observations to the tectonic framework of the Shillong Plateau.

The stratigraphic surface of the basement rocks, presumably once flat, is deformed in both north-south and east-west directions, giving an overall dome shape (Fig. 4). This deformation is clearly evident in plateau-top rivers that trace this stratigraphic contact (Fig. 8). Rosenkranz et al. (2018) also noted this feature of the drainage network and, based on the assumption that the channel network is transiently responding to uplift, suggested that the different elevations of major knickpoints below plateau-top channels evidences differential uplift of the southern plateau margin, with maximum uplift in the centre. We argue that, as the plateau-top channels simply represent a stratigraphic contact and the transient migration of knickpoints has been substantially complicated by layered lithologies

671 of varying erodibility, the channels cannot be used to infer active deformation of the
672 plateau surface or differential uplift. Whether the doming deformation of the stratigraphic
673 contact between basement rocks and the sediments occurred prior to the onset of
674 exhumation or is associated with the rise of the plateau remains an open question. The
675 linear margin of the southern Shillong Plateau is not definitive evidence for a surface-
676 rupturing plateau-bounding fault: the linearity of the margin's topography is also consistent
677 with the stripping of soft overlying strata along planar contacts under the south-vergent
678 monocline model (Clark and Bilham, 2008) (Fig. 12).

679

680 In the northwest, the topographic expression and geology of the Khri Scarp, which
681 delineates the northern boundary of the high-elevation low-topography plateau, lends itself
682 to interpretation as an active fault scarp. The scarp may be the topographic expression of
683 rupture on the Oldham fault, the existence of which was originally inferred based on re-
684 analysis of geodetic data (Bilham and England, 2001; England and Bilham, 2015).
685 Subsequently, its existence was supported by thermochronology studies (Clark and Bilham,
686 2008; Biswas et al, 2007) and topographic metrics such as normalized channel steepness
687 (Clark and Bilham, 2008) and incision depth (England and Bilham, 2015). Local steepening of
688 channels at the scarp revealed by the analysis of the χ profiles (Fig. 7b, 11a), despite no
689 lithological change, is consistent with the Khri scarp's interpretation as an active fault scarp.
690 In the northeast, basement rocks have been uplifted (Biswas et la., 2007; Clark and Bilham,
691 2008) and exposed (Fig. 2) on the Himalayan side of the Oldham fault suggesting that
692 movement on the Oldham fault is not the only tectonic deformation controlling Plateau
693 uplift to the north. The morphology of the northern plateau margin shows it is not

694 immediately bound by a single linear fault as in the south (see discussion in section 5.2),
695 suggesting the tectonic uplift is possibly accommodated by (e.g., Clark and Bilham, 2008): (i)
696 flexure of the crust across the Himalayan foreland, (ii) blind faulting at depth, or (iii) a
697 complex array of faults reaching the surface in the Brahmaputra valley sediments, the
698 topographic signature of which is readily erased by levelling processes in the soft alluvium or
699 episodic aggradation across the Brahmaputra valley.

700

701 ## 5.5. Implications for the evolution of the Shillong Plateau and the analysis of river long
702 profiles

703 The geomorphology of the Shillong Plateau shows that differences in lithological erodibility
704 in layered rocks can have dramatic effects on channel profile form, which can be inherited
705 even after the contrasting rocks are no longer preserved. Recent research has argued that
706 the contrast in rock erodibility between basement and sedimentary cover 'is not the
707 dominant factor responsible for the change from exhumation to surface uplift' and invoked
708 a tectonic driver instead (Govin et al., 2018). Govin et al. (2018) observe a ~3.5 Ma lag
709 between initiation of surface uplift and the moment basement rocks from the Shillong
710 Plateau become the primary sediment contributor to the sedimentary basin to the south
711 (after 1.5 Ma), which they interpret as evidence to support an increase in fault slip rate at
712 the end of the Miocene. However, we argue that exhumation of resistant basement rocks
713 can explain both modern morphology and the lag time between exhumation, surface uplift
714 and release of crystalline basement lithologies without requiring an increase in rock uplift
715 rate.

716

717 Firstly, recent modelling by Forte et al. (2016) shows that exhumation of a tilted contact
718 between a 'soft' lithology and its underlying 'hard' basement can lead to surface uplift and
719 spatial distribution of exposure consistent with observed patterns across the Shillong
720 Plateau. Their study shows that when the hard lithology is exposed over a given area, the
721 erosion rate drops over the area, which is what drives surface uplift. Therefore, the hard
722 lithology does not become a significant contributor of sediment to the sedimentary basin
723 until the erosion rate over the areas where it is exposed increases (see transition from "2-
724 3.5 Ma" to "present day" stages in Fig. 12): a delay between rock exposure and supply to
725 the basin is thus expected. In the model by Forte et al. (2016), the timescale over which
726 erosion rates across the hard lithology re-equilibrate to the uplift rates is on the order of
727 millions of years. We acknowledge that the modelling study is simplistic and not calibrated
728 to the Shillong Plateau, albeit performed on a similar scale. This result nevertheless offers a
729 mechanism which could contribute to the ~3.5 Ma delay between surface uplift and the
730 arrival of significant amounts of basement-derived sediment to the sedimentary basin to the
731 south. Secondly, we observe in places that the basement rocks are overlain by sedimentary
732 strata that are sufficiently durable to form scarp slopes and retain high topography (Fig. 5c).
733 Therefore, it is also possible that the initial growth of higher elevation topography did not
734 require full exposure of crystalline basement, but was initially driven by the increasing
735 exposure of the lowest part of the sedimentary cover that had been buried and gained great
736 rock strength. Such process could have delayed the emersion of the crystalline basement
737 and thus the delivery of basement-derived sediment to the basin to the south. Considering
738 this hardened sedimentary succession is up to 200 m thick in places, it seems reasonable to
739 expect a delay of a few millions of years between accelerated surface uplift and delivery of
740 basement clasts to the Surma Basin, given erosion rates of 0.05 to 0.1 mm/yr.

We argue that the channel profiles in the Shillong Plateau cannot be interpreted (in the style of Kirby and Whipple, 2001) as a record of uplift resulting from activity along the Dauki fault. Instead, the profiles primarily preserve information about stratigraphy. Therefore, when attempting to use river long profiles as records of uplift, it is important to consider not only the rocks the river is currently incising but also the rocks that have been incised in the past. This would require a firm evidence-based understanding of the relative erodibility of rocks, which remains outstanding, and detailed geological information about lithological packages which may no longer be preserved, thus presenting a challenge for future geomorphological studies.

6. Conclusions

The topographic character of the northern Shillong Plateau region is systematically different to that of the southern and central plateau. A zone of high steepness is observed in the lower reaches of northeast draining rivers, although there is not sufficient evidence to definitively attribute these knickzones to base level fall or lithological variation. The plateau boundary is highly irregular in plan-view, testifying to the active stripping followed by aggradation of sediment from the Brahmaputra valley; the Brahamputra River exerts a base level control on the rivers draining the northern edge of the Shillong Plateau. Catchment morphology and topography in the northern Shillong Plateau is dominantly controlled by the structure of basement rocks and the topographic features of the north-eastern region are reminiscent of stable cratonic interior landscapes. We favour a model where the topography and river profiles effectively represent a reactivated Mesozoic landscape,

764 consistent with burial in the late cretaceous and re-exposure by sediment stripping under
765 the present phase of exhumation which began in the Miocene.
766
767 The southern and central Shillong Plateau has been planated by the preferential erosion of
768 cover sediments along the contact with the basement, re-exposing a palaeosurface which is
769 expressed as the modern low relief surface of the Shillong Plateau. Scarp retreat towards
770 the plateau margins appears to be an important erosion mechanism, facilitating the
771 effective removal of sediments from the low gradient palaeosurface. The plateau margins
772 are fluvially dissected, generating > 1500 m of relief. Such high contrasts in steepness
773 within catchment networks appear to be facilitating the internal reorganisation of drainage
774 networks, as evidenced by river capture events. Our observations support recent work
775 documenting erosion rates in the steep, incised parts of the landscape (Rosenkranz et al.,
776 2018): despite record-breaking rainfall, erosion is very slow (~0.05-0.2 mm/yr) due to very
777 high erosion thresholds resulting from the mantling of the river bed by very large boulders.
778
779 We acknowledge that surface rupture of the Dauki Fault and/or an increase in fault slip rate
780 may explain (i) deep incision along the southern plateau margin, (ii) the lag time between
781 exhumation (beginning in the early Miocene) and surface uplift (initiating at the end of the
782 Miocene) of the Shillong Plateau, and (iii) the ~3.5 Ma lag time between the initiation of
783 surface uplift and the arrival of significant amounts of basement-derived sediment to the
784 sedimentary basin to the south. However, we argue that exhumation of the tilted basement
785 surface can explain all observations without recourse to changing fault slip rates, and that
786 indurated sedimentary rocks immediately above the basement may have delayed the arrival
787 of basement-derived sediment in the Surma basin. We propose that the surface slope of the

788 exposed basement contact is exerting a control on the spatial pattern of fluvial incision, with
789 headward retreat possibly moderated by low sediment fluxes from the plateau interior.
790 This model of landscape evolution, supported by insights from previous theoretical work,
791 neatly accounts for the spatial variations in topography, erosion rates, sedimentary cover
792 and incision depth observed in the Shillong Plateau.
793

794 Acknowledgements

795 SRTM 30 meter resolution topographic data was obtained from OpenTopography.org.
796 Software used for topographic analyses is available at
797 https://github.com/LSDtopotools/LSDTopoTools_ChiMudd2014, with instructions available
798 at https://lsdtopotools.github.io/LSDTT_documentation/LSDTT_chi_analysis.html. We are
799 very grateful to two anonymous reviewers whose comments and suggestions helped
800 improve the manuscript. We thank the editorial team at Meghalaya Rivers for additional
801 photographs of the field site.
802

803 Author contributions

804 CMS designed the project, carried out fieldwork and performed the analyses, with inputs
805 from MA, SMM and HDS. CMS wrote a first version of the paper with inputs from all authors.
806 MA, SMM and HDS produced the final version of the paper.
807

808 References

809 Attal, M., 2017. Linkage between sediment transport and supply in mountain rivers, in:
810 Gravel-Bed Rivers. Wiley-Blackwell, pp. 329–353.

811 Attal, M., Cowie, P.A., Whittaker, A.C., Hobley, D., Tucker, G.E., Roberts, G.P., 2011. Testing
812 fluvial erosion models using the transient response of bedrock rivers to tectonic forcing
813 in the Apennines, Italy. J. Geophys. Res.-Earth Surf. 116, F02005.
814 https://doi.org/10.1029/2010JF001875
815 Attal, M., Mudd, S.M., Hurst, M.D., Weinman, B., Yoo, K., Naylor, M., 2015. Impact of change
816 in erosion rate and landscape steepness on hillslope and fluvial sediments grain size in
817 the Feather River basin (Sierra Nevada, California). Earth Surf. Dyn. 3, 201–222.
818 https://doi.org/10.5194/esurf-3-201-2015
819 Banerjee, P., Buergmann, R., Nagarajan, B., Apel, E., 2008. Intraplate deformation of the
820 Indian subcontinent. Geophys. Res. Lett. 35, L18301.
821 https://doi.org/10.1029/2008GL035468
822 Berkelhammer, M., Sinha, A., Stott, L., Cheng, H., Pausata, F.S.R., Yoshimura, K., 2012. An
823 Abrupt Shift in the Indian Monsoon 4000 Years Ago, in: Giosan, L., Fuller, D.Q., Nicoll, K.,
824 Flad, R.K., Clift, P.D. (Eds.), Climates, Landscapes, and Civilizations. Amer Geophysical
825 Union, Washington, pp. 75–87.
826 Bilham, R., England, P., 2001. Plateau “pop-up” in the great 1897 Assam earthquake. Nature
827 410, 806–809. https://doi.org/10.1038/35071057
828 Biswas, S., Coutand, I., Grujic, D., Hager, C., Stoeckli, D., Grasemann, B., 2007. Exhumation
829 and uplift of the Shillong plateau and its influence on the eastern Himalayas: New
830 constraints from apatite and zircon (U-Th-[Sm])/He and apatite fission track analyses.
831 Tectonics 26, TC6013. https://doi.org/10.1029/2007TC002125
832 Biswas, S., Grasemann, B., 2005. Quantitative morphotectonics of the southern Shillong
833 Plateau (Bangladesh/India). Austrian Journal of Earth Sciences 97, 82–93.

834 Bookhagen, B., Burbank, D.W., 2010. Toward a complete Himalayan hydrological budget:
835 Spatiotemporal distribution of snowmelt and rainfall and their impact on river discharge.
836 J. Geophys. Res.-Earth Surf. 115, F03019. https://doi.org/10.1029/2009JF001426
837 Bookhagen, B., Burbank, D.W., 2006. Topography, relief, and TRMM-derived rainfall
838 variations along the Himalaya. Geophys. Res. Lett. 33, L13402.
839 https://doi.org/10.1029/2006GL026944
840 Braun, J., Guillocheau, F., Robin, C., Baby, G., Jelsma, H., 2014. Rapid erosion of the Southern
841 African Plateau as it climbs over a mantle superswell. J. Geophys. Res.-Solid Earth 119,
842 6093–6112. https://doi.org/10.1002/2014JB010998
843 Brocard, G.Y., Willenbring, J.K., Miller, T.E., Scatena, F.N., 2016. Relict landscape resistance
844 to dissection by upstream migrating knickpoints. J. Geophys. Res.-Earth Surf. 121, 1182–
845 1203. https://doi.org/10.1002/2015JF003678
846 Bufe, A., Paola, C. and Burbank, D.W., 2016. Fluvial bevelling of topography controlled by
847 lateral channel mobility and uplift rate. Nat. Geosci. *9*, 706.
848 https://doi.org/10.1038/ngeo2773
849 Castelltort, S., Goren, L., Willett, S.D., Champagnac, J.-D., Herman, F., Braun, J., 2012. River
850 drainage patterns in the New Zealand Alps primarily controlled by plate tectonic strain.
851 Nat. Geosci. 5, 744–748. https://doi.org/10.1038/NGEO1582
852 Clark, M.K., Bilham, R., 2008. Miocene rise of the Shillong Plateau and the beginning of the
853 end for the Eastern Himalaya. Earth Planet. Sci. Lett. 269, 336–350.
854 https://doi.org/10.1016/j.epsl.2008.01.045
855 Cook, K.L., Andermann, C., Gimbert, F., Adhikari, B.R. and Hovius, N., 2018. Glacial lake
856 outburst floods as drivers of fluvial erosion in the Himalaya. Science, 362(6410), pp. 53-
857 57. https://doi.org/10.1126/science.aat4981

858 Das, J., Saraf, A., Jain, A., 1995. Fault Tectonics of the Shillong Plateau and Adjoining Regions,
859 Northeast India Using Remote-Sensing Data. Int. J. Remote Sens. 16, 1633–1646.
860 https://doi.org/10.1080/01431169508954501
861 de Carvalho Junior, O.A., Guimaraes, R.F., Martins, E. de S., Trancoso Gomes, R.A., 2015.
862 Chapada dos Veadeiros: The Highest Landscapes in the Brazilian Central Plateau, in:
863 Vieira, B.C., Salgado, A. a. R., Santos, L.J.C. (Eds.), Landscapes and Landforms of Brazil.
864 Springer, Dordrecht, pp. 221–230.
865 Dettman, D.L., Kohn, M.J., Quade, J., Ryerson, F.J., Ojha, T.P., Hamidullah, S., 2001. Seasonal
866 stable isotope evidence for a strong Asian monsoon throughout the past 10.7 m.y.
867 Geology 29, 31–34. https://doi.org/10.1130/0091-
868 7613(2001)029<0031:SSIEFA>2.0.CO;2
869 DiBiase, R.A., Whipple, K.X., Heimsath, A.M., Ouimet, W.B., 2010. Landscape form and
870 millennial erosion rates in the San Gabriel Mountains, CA. Earth Planet. Sci. Lett. 289,
871 134–144. https://doi.org/10.1016/j.epsl.2009.10.036
872 Duarah, B.P., Phukan, S., 2011. Understanding the Tectonic Behaviour of the Shillong
873 Plateau, India using Remote Sensing Data. J. Geol. Soc. India 77, 105–112.
874 https://doi.org/10.1007/s12594-011-0013-8
875 Dutt, S., Gupta, A.K., Clemens, S.C., Cheng, H., Singh, R.K., Kathayat, G., Edwards, R.L., 2015.
876 Abrupt changes in Indian summer monsoon strength during 33,800 to 5500years BP.
877 Geophys. Res. Lett. 42, 5526–5532. https://doi.org/10.1002/2015GL064015
878 England, P., Bilham, R., 2015. The Shillong Plateau and the great 1897 Assam earthquake.
879 Tectonics 34, 1792–1812. https://doi.org/10.1002/2015TC003902
880 Flint, J., 1974. Stream Gradient as a Function of Order, Magnitude, and Discharge. Water
881 Resour. Res. 10, 969–973. https://doi.org/10.1029/WR010i005p00969

882 Forte, A.M., Yanites, B.J., Whipple, K.X., 2016. Complexities of landscape evolution during
883 incision through layered stratigraphy with contrasts in rock strength. Earth Surf. Process.
884 Landf. 41, 1736–1757. https://doi.org/10.1002/esp.3947
885 Giachetta, E., Refice, A., Capolongo, D., Gasparini, N.M., Pazzaglia, F.J., 2014. Orogen-scale
886 drainage network evolution and response to erodibility changes: insights from
887 numerical experiments. Earth Surf. Process. Landf. 39, 1259–1268.
888 https://doi.org/10.1002/esp.3579
889 Gilbert, G.K., 1877. Report on the Geology of the Henry Mountains. U.S. Government
890 Printing Office, Washington, D. C.
891 Goren, L., Castelltort, S., Klinger, Y., 2015. Modes and rates of horizontal deformation from
892 rotated river basins: Application to the Dead Sea fault system in Lebanon. Geology 43,
893 843–846. https://doi.org/10.1130/G36841.1
894 Govin, G., Najman, Y., Copley, A., Millar, I., van der Beek, P., Huyghe, P., Grujic, D.,
895 Davenport, J., 2018. Timing and mechanism of the rise of the Shillong Plateau in the
896 Himalayan foreland. Geology 46, 279–282. https://doi.org/10.1130/G39864.1
897 Grujic, D., Coutand, I., Bookhagen, B., Bonnet, S., Blythe, A., Duncan, C., 2006. Climatic
898 forcing of erosion, landscape, and tectonics in the Bhutan Himalayas. Geology 34, 801–
899 804. https://doi.org/10.1130/G22648.1
900 Gupta, R.P., Sen, A.K., 1988. Imprints of the Ninety-East Ridge in the Shillong Plateau, Indian
901 Shield. Tectonophysics 154, 335–341. https://doi.org/10.1016/0040-1951(88)90111-4
902 Hack, J.T., 1957. Studies of Longitudinal Stream Profiles in Virginia and Maryland, US
903 Geological Survey Professional Paper. U.S. Government Printing Office, Washington, D.
904 C.

905 Hallet, B., Molnar, P., 2001. Distorted drainage basins as markers of crustal strain east of the
906 Himalaya. J. Geophys. Res.-Solid Earth 106, 13697–13709.
907 https://doi.org/10.1029/2000JB900335
908 Harel, M.-A., Mudd, S.M., Attal, M., 2016. Global analysis of the stream power law
909 parameters based on worldwide Be-10 denudation rates. Geomorphology 268, 184–196.
910 https://doi.org/10.1016/j.geomorph.2016.05.035
911 Howard, A., Dietrich, W., Seidl, M., 1994. Modeling Fluvial Erosion on Regional to
912 Continental Scales. J. Geophys. Res.-Solid Earth 99, 13971–13986.
913 https://doi.org/10.1029/94JB00744
914 Howard, A., Kerby, G., 1983. Channel Changes in Badlands. Geol. Soc. Am. Bull. 94, 739–752.
915 https://doi.org/10.1130/0016-7606(1983)94<739:CCIB>2.0.CO;2
916 Johnson, S., Alam, A., 1991. Sedimentation and Tectonics of the Sylhet Trough, Bangladesh.
917 Geol. Soc. Am. Bull. 103, 1513–1527. https://doi.org/10.1130/0016-
918 7606(1991)103<1513:SATOTS>2.3.CO;2
919 Kayal, J.R., Arefiev, S.S., Baruah, S., Hazarika, D., Gogoi, N., Gautam, J.L., Baruah, S., Dorbath,
920 C., Tatevossian, R., 2012. Large and great earthquakes in the Shillong plateau-Assam
921 valley area of Northeast India Region: Pop-up and transverse tectonics. Tectonophysics
922 532, 186–192. https://doi.org/10.1016/j.tecto.2012.02.007
923 Kirby, E., Whipple, K., 2001. Quantifying differential rock-uplift rates via stream profile
924 analysis. Geology 29, 415–418. https://doi.org/10.1130/0091-
925 7613(2001)029<0415:QDRURV>2.0.CO;2
926 Kirby, E., Whipple, K.X., 2012. Expression of active tectonics in erosional landscapes. J. Struct.
927 Geol. 44, 54–75. https://doi.org/10.1016/j.jsg.2012.07.009

928 Kumar, A., Mitra, S., Suresh, G., 2015. Seismotectonics of the eastern Himalayan and indo-
929 burman plate boundary systems. Tectonics 34, 2279–2295.
930 https://doi.org/10.1002/2015TC003979
931 Mandal, S.K., Lupker, M., Burg, J.-P., Valla, P.G., Haghipour, N., Christl, M., 2015. Spatial
932 variability of Be-10-derived erosion rates across the southern Peninsular Indian
933 escarpment: A key to landscape evolution across passive margins. Earth Planet. Sci. Lett.
934 425, 154–167. https://doi.org/10.1016/j.epsl.2015.05.050
935 Mecchia, M., Sauro, F., Piccini, L., De Waele, J., Sanna, L., Tisato, N., Lira, J., Vergara, F., 2014.
936 Geochemistry of surface and subsurface waters in quartz-sandstones: significance for
937 the geomorphic evolution of tepui table mountains (Gran Sabana, Venezuela). J. Hydrol.
938 511, 117–138. https://doi.org/10.1016/j.jhydrol.2014.01.029
939 Migon, P., Prokop, P., 2013. Landforms and landscape evolution in the Mylliem Granite Area,
940 Meghalaya Plateau, Northeast India. Singap. J. Trop. Geogr. 34, 206–228.
941 https://doi.org/10.1111/sjtg.12025
942 Miller, S.R., Slingerland, R.L., Kirby, E., 2007. Characteristics of steady state fluvial
943 topography above fault-bend folds. J. Geophys. Res.-Earth Surf. 112, F04004.
944 https://doi.org/10.1029/2007JF000772
945 Milliman, J., Syvitski, J., 1992. Geomorphic Tectonic Control of Sediment Discharge to the
946 Ocean - the Importance of Small Mountainous Rivers. J. Geol. 100, 525–544.
947 https://doi.org/10.1086/629606
948 Mitra, S., Priestley, K., Bhattacharyya, A.K., Gaur, V.K., 2005. Crustal structure and
949 earthquake focal depths beneath northeastern India and southern Tibet. Geophys. J. Int.
950 160, 227–248. https://doi.org/10.1111/j.1365-246X.2004.02470.x

951 Morisawa, M.E., 1962. Quantitative Geomorphology of Some Watersheds in the
952 Appalachian Plateau. GSA Bulletin 73, 1025–1046. https://doi.org/10.1130/0016-
953 7606(1962)73[1025:QGOSWI]2.0.CO;2
954 Mudd, S.M., Attal, M., Milodowski, D.T., Grieve, S.W.D., Valters, D.A., 2014. A statistical
955 framework to quantify spatial variation in channel gradients using the integral method
956 of channel profile analysis. J. Geophys. Res. Earth Surf. 119, 2013JF002981.
957 https://doi.org/10.1002/2013JF002981
958 Mudd, S.M., Clubb, F.J., Gailleton, B., Hurst, M.D., 2018. How concave are river channels?
959 Earth Surface Dynamics 6, 505–523. https://doi.org/https://doi.org/10.5194/esurf-6-
960 505-2018
961 Mukherjee, P.K., Punj, N.K., Behera, U.K., Borah., A.C., 2012. District Resource Map, East
962 Khasi Hills, Meghalaya. Geol. Surv. India.
963 Mukherjee, P.K., Punj, N.K., Behera, U.K., Borah., A.C., 2012. District Resource Map, West
964 Khasi Hills, Meghalaya. Geol. Surv. India.
965 Mukherjee, P.K., Raghupathy, M., Sahu, B.K., Singh, H., Borah., A.C., Roy, B., 2013. District
966 Resource Map, West Garo Hills, Meghalaya. Geol. Surv. India.
967 Mukherjee, P.K., Punj, N.K., Behera, U.K., Borah., A.C., Roy, B., 2013. District Resource Map,
968 South Garo Hills, Meghalaya. Geol. Surv. India.
969 Mukherjee, P.K., Punj, N.K., Raghupathy, M., Sahu, B.K., Singh, H., Borah., A.C., Roy, B., 2013.
970 District Resource Map, Ri - Bhoi District, Meghalaya. Geol. Surv. India.
971 Mukherjee, P.K., Sahu, B.K., Singh, H., Borah., A.C., 2014. District Resource Map, Jaintia Hills,
972 Meghalaya. Geol. Surv. India.

973 Murata, F., Hayashi, T., Matsumoto, J., Asada, H., 2007. Rainfall on the Meghalaya plateau in
974 northeastern India - one of the rainiest places in the world. Nat. Hazards 42, 391–399.
975 https://doi.org/10.1007/s11069-006-9084-z
976 Najman, Y., Bracciali, L., Parrish, R.R., Chisty, E., Copley, A., 2016. Evolving strain partitioning
977 in the Eastern Himalaya: The growth of the Shillong Plateau. Earth Planet. Sci. Lett. 433,
978 1–9. https://doi.org/10.1016/j.epsl.2015.10.017
979 Oldham, R.D., 1899. Report on the great earthquake of 12 June 1897. Mem. Geol. Surv.
980 India 29, 1–379.
981 Orme, A.R., 2007. The rise and fall of the Davisian cycle of erosion: Prelude, fugue, coda, and
982 sequel. Phys. Geogr. 28, 474–506. https://doi.org/10.2747/0272-3646.28.6.474
983 Ouimet, W.B., Whipple, K.X., Granger, D.E., 2009. Beyond threshold hillslopes: Channel
984 adjustment to base-level fall in tectonically active mountain ranges. Geology 37, 579–
985 582. https://doi.org/10.1130/G30013A.1
986 Perron, J.T., Royden, L., 2013. An integral approach to bedrock river profile analysis. Earth
987 Surf. Process. Landforms 38, 570–576. https://doi.org/10.1002/esp.3302
988 Peulvast, J.-P., Betard, F., 2015. A history of basin inversion, scarp retreat and shallow
989 denudation: The Araripe basin as a keystone for understanding long-term landscape
990 evolution in NE Brazil. Geomorphology 233, 20–40.
991 https://doi.org/10.1016/j.geomorph.2014.10.009
992 Piccini, L., Mecchia, M., 2009. Solution weathering rate and origin of karst landforms and
993 caves in the quartzite of Auyan-tepui (Gran Sabana, Venezuela). Geomorphology 106,
994 15–25. https://doi.org/10.1016/j.geomorph.2008.09.019
995 Prokop, P., 2014. The Meghalaya Plateau: Landscapes in the Abode of the C ouds, in: Kale,
996 V.S. (Ed.), Landscapes and Landforms of India. Springer, Dordrecht, pp. 173–180.

997 Rajendran, C.P., Rajendran, K., Duarah, B.P., Baruah, S., Earnest, A., 2004. Interpreting the
998 style of faulting and paleoseismicity associated with the 1897 Shillong, northeast India,
999 earthquake: Implications for regional tectonism. Tectonics 23, TC4009.
1000 https://doi.org/10.1029/2003TC001605
1001 Rosenkranz, R., Schildgen, T., Wittmann, H., Spiegel, C., 2018. Coupling erosion and
1002 topographic development in the rainiest place on Earth: Reconstructing the Shillong
1003 Plateau uplift history with in-situ cosmogenic Be-10. Earth Planet. Sci. Lett. 483, 39–51.
1004 https://doi.org/10.1016/j.epsl.2017.11.047
1005 Royden, L., Clark, M.K., Whipple, K.X., 2000. Evolution of River Elevation Profiles by Bedrock
1006 Incision: Analytical Solutions for Transient River Profiles Related to Changing Uplift and
1007 Precipitation Rates. Eos Trans. AGU 81, Fall Meet. Suppl., Abstract T62F-09.
1008 Sarma, J.N., 2005. Fluvial process and morphology of the Brahmaputra River in Assam, India.
1009 Geomorphology 70, 226–256. https://doi.org/10.1016/j.geomorph.2005.02.007
1010 Scherler Dirk, Bookhagen Bodo, Strecker Manfred R., 2014. Tectonic control on
1011 10Be-derived erosion rates in the Garhwal Himalaya, India. Journal of Geophysical
1012 Research: Earth Surface 119, 83–105. https://doi.org/10.1002/2013JF002955
1013 Schmidt, K., 1989. The Significance of Scarp Retreat for Cenozoic Landform Evolution on the
1014 Colorado Plateau, USA. Earth Surf. Process. Landf. 14, 93–105.
1015 https://doi.org/10.1002/esp.3290140202
1016 Schwanghart, W., Bernhardt, A., Stolle, A., Hoelzmann, P., Adhikari, B.R., Andermann, C.,
1017 Tofelde, S., Merchel, S., Rugel, G., Fort, M., Korup, O., 2016. Repeated catastrophic
1018 valley infill following medieval earthquakes in the Nepal Himalaya. Science 351, 147–
1019 150. https://doi.org/10.1126/science.aac9865

1020 Shobe, C.M., Tucker, G.E., Rossi, M.W., 2018. Variable-threshold behavior in rivers arising
1021 from hillslope-derived blocks. Journal of Geophysical Research: Earth Surface in press.
1022 https://doi.org/10.1029/2017JF004575
1023 Sklar, L., Dietrich, W.E., 1998. River Longitudinal Profiles and Bedrock Incision Models:
1024 Stream Power and the Influence of Sediment Supply, in: Rivers Over Rock: Fluvial
1025 Processes in Bedrock Channels. American Geophysical Union (AGU), pp. 237–260.
1026 Sklar, L.S., Dietrich, W.E., 2004. A mechanistic model for river incision into bedrock by
1027 saltating bed load. Water Resour. Res. 40, W06301.
1028 https://doi.org/10.1029/2003WR002496
1029 Sklar, L.S., Dietrich, W.E., 2001. Sediment and rock strength controls on river incision into
1030 bedrock. Geology 29, 1087–1090. https://doi.org/10.1130/0091-
1031 7613(2001)029<1087:SARSCO>2.0.CO;2
1032 Snyder, N.P., Whipple, K.X., Tucker, G.E., Merritts, D.J., 2003. Channel response to tectonic
1033 forcing: field analysis of stream morphology and hydrology in the Mendocino triple
1034 junction region, northern California. Geomorphology 53, 97–127.
1035 https://doi.org/10.1016/S0169-555X(02)00349-5
1036 Stock, J.D., Montgomery, D.R., 1999. Geologic constraints on bedrock river incision using the
1037 stream power law. J. Geophys. Res.-Solid Earth 104, 4983–4993.
1038 https://doi.org/10.1029/98JB02139
1039 Sukhija, B.S., Rao, M.N., Reddy, D.V., Nagabhushanam, P., Hussain, S., Chadha, R.K., Gupta,
1040 H.K., 1999. Timing and return period of major palaeoseismic events in the Shillong
1041 Plateau, India. Tectonophysics 308, 53–65. https://doi.org/10.1016/S0040-
1042 1951(99)00082-7

1043 Tucker, G.E., Lancaster, S., Gasparini, N., Bras, R., 2001. The Channel-Hillslope Integrated
1044 Landscape Development Model (CHILD), in: Landscape Erosion and Evolution Modeling.
1045 Springer, Boston, MA, pp. 349–388.
1046 Twidale, C.R., 1992. King of the plains: Lester King's contributions to geomorphology.
1047 Geomorphology 5, 491–509. https://doi.org/10.1016/0169-555X(92)90021-F
1048 Vernant, P., Bilham, R., Szeliga, W., Drupka, D., Kalita, S., Bhattacharyya, A.K., Gaur, V.K.,
1049 Pelgay, P., Cattin, R., Berthet, T., 2014. Clockwise rotation of the Brahmaputra Valley
1050 relative to India: Tectonic convergence in the eastern Himalaya, Naga Hills, and Shillong
1051 Plateau. J. Geophys. Res.-Solid Earth 119, 6558–6571.
1052 https://doi.org/10.1002/2014JB011196
1053 Whipple, K.X., DiBiase, R.A., Ouimet, W.B., Forte, A.M., 2017. Preservation or piracy:
1054 Diagnosing low-relief, high-elevation surface formation mechanisms. Geology 45, 91–94.
1055 https://doi.org/10.1130/G38490.1
1056 Whipple, K.X., Forte A. M., DiBiase R. A., Gasparini N. M., Ouimet W. B., 2017. Timescales of
1057 landscape response to divide migration and drainage capture: Implications for the role
1058 of divide mobility in landscape evolution. Journal of Geophysical Research: Earth Surface
1059 122, 248–273. https://doi.org/10.1002/2016JF003973
1060 Whittaker, A.C., Attal, M., Cowie, P.A., Tucker, G.E., Roberts, G., 2008. Decoding temporal
1061 and spatial patterns of fault uplift using transient river long profiles. Geomorphology
1062 100, 506–526. https://doi.org/10.1016/j.geomorph.2008.01.018
1063 Willett, S.D., McCoy, S.W., Perron, J.T., Goren, L., Chen, C.-Y., 2014. Dynamic Reorganization
1064 of River Basins. Science 343, 1117–+. https://doi.org/10.1126/science.1248765
1065 Wobus, C., Whipple, K.X., Kirby, E., Snyder, N., Johnson, J., Spyropolou, K., Crosby, B.,
1066 Sheehan, D., 2006. Tectonics from topography: Procedures, promise, and pitfalls, in:

Special Paper 398: Tectonics, Climate, and Landscape Evolution. Geological Society of America, pp. 55–74.

Wray, R.A.L., 2009. The Gran Sabana: The World's Finest Quartzite Karst?, Geomorphological Landscapes of the World. Springer-Verlag Berlin, Berlin.

Yin, A., Dubey, C.S., Webb, A. a. G., Kelty, T.K., Grove, M., Gehrels, G.E., Burgess, W.P., 2010. Geologic correlation of the Himalayan orogen and Indian craton: Part 1. Structural geology, U-Pb zircon geochronology, and tectonic evolution of the Shillong Plateau and its neighboring regions in NE India. Geol. Soc. Am. Bull. 122, 336–359. https://doi.org/10.1130/B26460.1

Figure caption

Figure 1: Topographic map and swath profiles of the Shillong Plateau. ~30 m resolution data from the Shuttle Radar Topography Mission (SRTM) were used. Northing and Easting (in km) is UTM WGS 1984 Zone 46N. Location of swaths is indicated by dashed boxes on the map. Major structural features, scarps (discussed in text) and location of photos (stars with corresponding figure labelled in italics) and cross-sections are indicated.

Figure 2: (**a**) Schematic geological map of the Shillong Plateau and surrounding area, adapted from Mukherjee et al., 2012a, 2012b, 2013a, 2013b, 2013c, 2014, Clark and Bilham, 2008, Yin et al., 2010, and Prokop, 2014. MFT, MBT and MCT are major Himalayan thrust faults: Main Frontal Thrust, Main Boundary Thrust and Main Central Thrust, respectively. BTSZ is the Badapani-Tyrsad Shear Zone . 'Shillong group' rocks are meta-sedimentary (quartzite, schist, conglomerate). Circled X and Y represent tips of the section shown in B.

(For interpretation of the references to colour in this figure legend, the reader is referred to the web version of this article.) (**b**) North-South (X-Y) crustal cross-section adapted from Biswas et al., 2007. Upward and downward block arrows represent areas of uplift and subsidence, respectively. Dark grey represents post-Cretaceous sediment; white is metamorphic and igneous basement. Light grey and vertical hash represent minimum and maximum thickness of cover removed by erosion, respectively, derived from thermochronological data (Biswas et al., 2007).

Figure 3: Catchment map of major catchments draining the Shillong Plateau. Not all local river names are known, but known names are 3: Wah Khri; 4: Umtrew; 6: Umiam; 7: Umkhen; 8: Wah Blei; 9: Kynshi; 10: Um Rilang; 11: Umngi; 12: Umiew; 13: Umraw; 14: Umngot (known as the Dauki River after crossing the Bangladesh border); 15: Myntdu. Catchment shadings distinguish between western catchments (1, 8, 9), northern and north-eastern catchments (2-4 and 5-7), and southern catchments (10-15).

Figure 4: Topographic profiles highlighting the differences in character of topographic relief between the southern (top) and northern (bottom) plateau regions. Profiles are located on Fig. 1 (indicated by letters with subscript).

Figure 5: Landscape photographs illustrating the Shillong Plateau's geomorphology. All pictures are from the southern part of the plateau (location of photographs in Fig. 1). (**a**) A planated plateau surface (foreground and horizon) formed along a stratigraphic level in cretaceous cover sediments with a deeply incised valley visible in the background. (**b**) Amphitheatre headwall of a fluvial channel, showing topographic expression of contrast in

rock resistance to erosion. (**c**) View looking down the lower Kynshi River (below the confluence of basins #8 and #9) with the ridgeline of the Kynshi scarp visible in the background. The valley at this location approximately corresponds to the valley incised in basement rocks in the centre of the cross section in Fig. 10c. All photos by Joe Rea-Dickins, 2016.

Figure 6: Drainage stability in the Shillong Plateau. (**a**) χ map of the southern Shillong Plateau. Differences in χ values can be seen in multiple places across drainage divides, in particular on north-facing scarps in the south of the larger catchments. Red arrow shows approximate viewpoint for the Google Earth imagery in panel (**b**), with potential capture sites indicated with red stars. (**b**) Google Earth imagery showing contrast in relief between plateau top and incised channels, and two potential capture sites characterised by low relief saddles (stars). White arrows show structurally entrained drainage while white triangles point towards potentially reverted drainage directions as a result of rapid incision by aggressor channels (red arrows). Distance from eastern capture site (star) to the edge of the plateau is indicated for scale (~6 km).

Figure 7: (**a**) χ map on hillshade for major basins of the Shillong Plateau. Differences in χ coordinate at drainage divides may reflect disequilibrium and potential drainage migration, with the "aggressor" and "victim" catchments characterised by the lowest and highest χ values, respectively (Willett et al., 2014). Disequilibrium seems to occur only locally, e.g., in the narrowest stretch of the Umiam catchment (#6) and on the eastern boundary of the Umngot catchment (#14). (**b**) Map of normalised steepness index k_{sn} on hillshade for major basins of the Shillong Plateau. Colour scale for k_{sn} is logarithmic, with brighter colours

representing steeper channels. ~30 m resolution data from the Shuttle Radar Topography Mission (SRTM). Northing and Easting (in km) is UTM WGS 1984 Zone 46N. In this figure, threshold area for a channel is 1.75 km^2.

Figure 8: χ plots of the western (**a**) and southern channels (**b, c**). Basin numbers correspond to Figure 3. The χ plots were generated using θ = 0.5 and A_0 = 1 m^2. Profiles are coloured according to the normalised steepness index k_{sn}, with brighter colours representing steeper channels. Note the clear contrast in steepness between plateau-top and incised channels, as well as the doming shown by the decrease in elevation of plateau top channels away from the centre of the area (eastward and westward from basin #12).

Figure 9: Photographs illustrating the morphology of rivers draining the southern margin of the Shillong Plateau (location of photographs in Fig. 1). Kayaks for scale are approximately 2-3 m long. (**a**) Mixed boulder/bedrock channel in the Umngot River (#14) with fluvial scouring. (**b**) Mixed boulder/bedrock channel formed of basement rocks in the upper Kynshi River (#9). Note the relatively low gradient, low entrenchment and limited bank scouring in this plateau-top channel. (**c**) Dramatic high-water scour lines from monsoon flows on the lower Kynshi River (below the confluence of basins #8 and #9), 10-15 meters above low flow water level. (**d**) Large boulders in the Kynshi River (#9). (**e**) In-situ scoured and potholed boulders in the Umsong River (#14). (**f**) Large boulder in the channel of the Kynshi River showing un-abraded surfaces, testifying to its relatively recent arrival in the channel via rockfall / landsliding. Photographs by Zorba Laloo (a,b), Banshan Kharkonger (c), Chris Korbulic (d,f) and Dan Rea-Dickins (e).

Figure 10: (**a**) Modelled topography and geology resulting from fluvial and hillslope erosion using the LithoCHILD model, adapted from Forte et al., 2016 (their Fig. 4C). In their model, erodible rocks overly basement rocks that are five times more resistant to erosion; in this scenario, the contact between the two units dips 5^{o} toward the south. This figure shows model result after 1.6 Ma, when most of the top erodible layer has been eroded away. (**b**) Remnant patches of sedimentary cover rocks overlying crystalline basement in the central part of the southern Shillong Plateau (from geological maps produced by the Geological Survey of India (GSI) (Mukherjee et al., 2012a, 2012b, 2013a, 2013b, 2013c, 2014); the patterns show similarities with the model results in (**a)**. The X'-Y' line represents the trace of the cross-section (**c**). (**c**) Geological cross-section X'-Y' illustrating the veneer of cover sediments left on a planar basement contact following the stripping of sedimentary strata. The cross-section was built using information (contacts, strike and dip of contacts) recorded in maps produced by the GSI (Mukherjee et al., 2012a; 2012b; 2013a; 2013b; 2013c; 2014). The north-facing scarp made of Cretaceous sediment is the Kynshi scarp. Note vertical exaggeration (dip of contacts is ~5^{o}).

Figure 11: χ plots of the northern (**a**) and north-eastern channels (**b**). Basin numbers correspond to Fig. 3. The χ plots were generated using $\theta = 0.5$ and $A_0 = 1$ m^2. Profiles are coloured according to the normalised steepness index k_{sn}, with brighter colours representing steeper channels.

Figure 12: Schematic block diagrams illustrating potential geomorphic evolution of the southern margin of the Shillong Plateau based on our analysis. Displayed are two interpretative progressions of landscape evolution through time, each illustrating a different

end-member tectonic hypothesis: a surface rupturing Dauki fault (left) (e.g. "pop-up" model of Bilham and England, 2001) versus a large scale south-vergent monocline (right) (e.g. Clark and Bilham, 2008). Note that the current landscape form and its evolution are displayed as being broadly similar under both tectonic end-member models as the incision signal is interpreted here as a consequence of the exhumation of the interface between the sedimentary cover and the more resistant basement. Landscapes with uniform relief are expected to be generated when one lithology is exposed at the surface for a time long enough to reach equilibrium.

Evidence	**Onset of rock uplift**	**Onset of surface uplift**	**Author(s)**
Stratigraphic, sedimentological, and petrographic analysis of the Shylet Trough sedimentary archive	23-5 Ma (Miocene)	5-2 Ma	Johnson and Alam, 1991
Apatite and zircon (U-Th-[Sm])/He and apatite fission track thermochronology	15-9 Ma	4-~3 Ma	Biswas et al., 2007
Apatite (U-Th-Sm)/He thermochronology	14-8 Ma	n/a	Clark and Bilham, 2008
Flexural subsidence modelling of the Shylet Trough sedimentary basin	n/a	3.5-~2 Ma	Najman et al., 2016
Erosion rates from detrital cosmogenic nuclide analysis and reconstruction of eroded volumes from topography	n/a	5-3 Ma	Rosenkranz et al., 2015
Dating of redirection of the palaeo-Brahmaputra River using the Himalayan foreland basin sedimentary record	n/a	5.2-4.9 Ma	Govin et al., 2018

Table 1: Summary of recent work temporally constraining the uplift history of the Shillong Plateau. Note the differentiation between onset of rock uplift (exhumation) and onset of surface uplift (when erosion rates fall behind rock uplift rates).

Fig. 1 (Color)

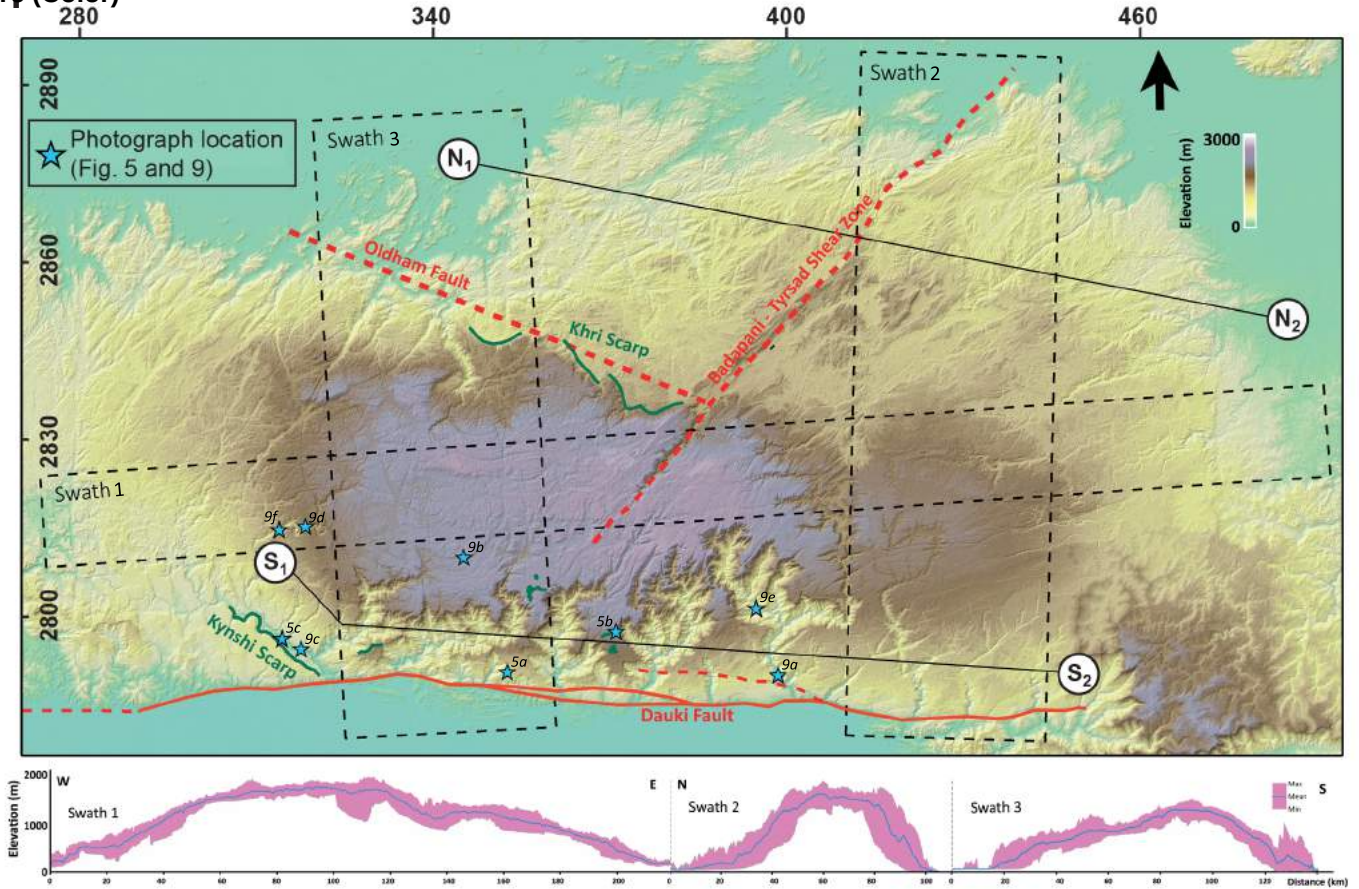
280
340
400
460
2890
2860
2830
2800
Photograph location (Fig. 5 and 9)
Swath 1
Swath 2
Swath 3
N1
N2
S1
S2
Oldham Fault
Khri Scarp
Badapani - Tyrsad Shear Zone
Kynshi Scarp
Dauki Fault
9f
9d
9b
9e
5b
5c
9c
5a
9a
Elevation (m)
3000
0
W
E
N
S
Swath 1
Swath 2
Swath 3
2000
1000
0
Distance (km)

Fig. 2

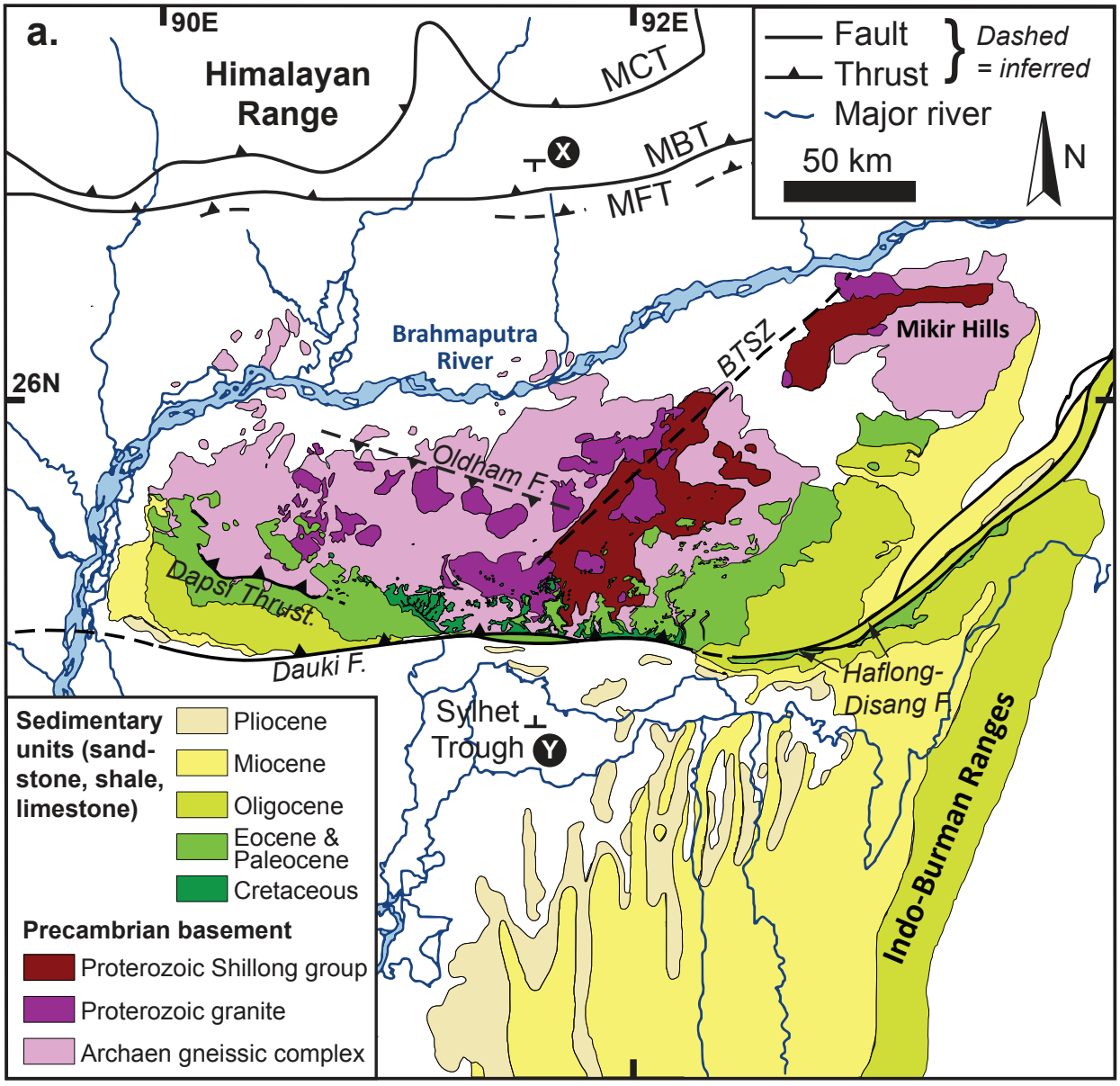
a.
90E
92E
Himalayan Range
MCT
MBT
MFT
X
Fault
Thrust
Major river
Dashed = inferred
50 km
N
Brahmaputra River
BTSZ
Mikir Hills
26N
Oldham F.
Dapsi Thrust
Dauki F.
Haflong-Disang F.
Sylhet Trough
Y
Indo-Burman Ranges
Sedimentary units (sand-stone, shale, limestone)
Pliocene
Miocene
Oligocene
Eocene & Paleocene
Cretaceous
Precambrian basement
Proterozoic Shillong group
Proterozoic granite
Archaen gneissic complex

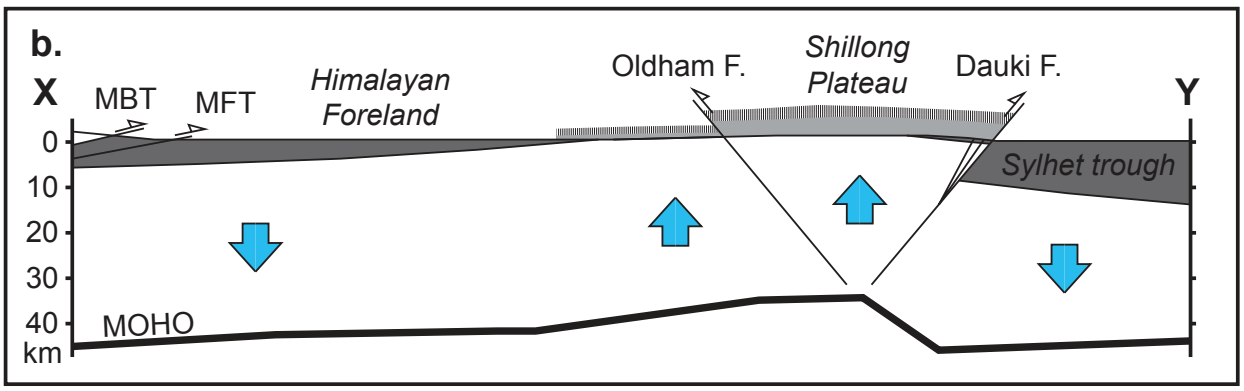
b.
X
MBT
MFT
Himalayan Foreland
Oldham F.
Shillong Plateau
Dauki F.
Y
0
10
20
30
40
km
Sylhet trough
MOHO

Fig. 3

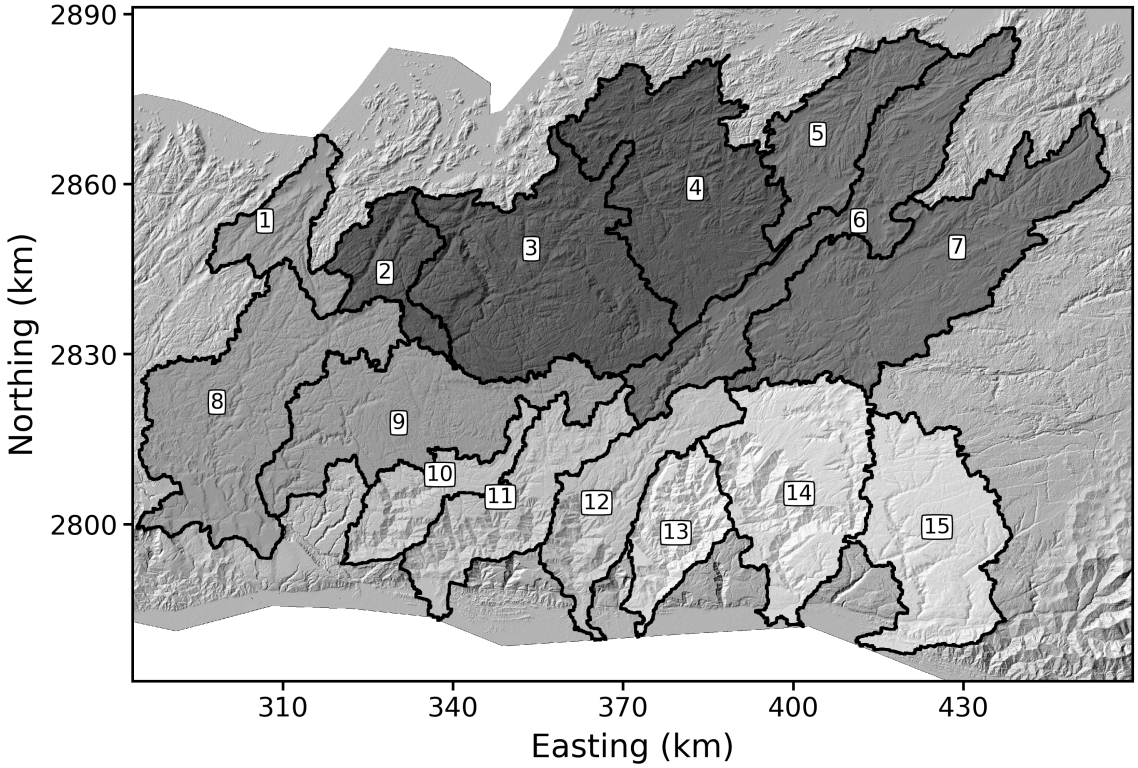
2890
2860
2830
2800
Northing (km)
310
340
370
400
430
Easting (km)
1
2
3
4
5
6
7
8
9
10
11
12
13
14
15

Fig. 4

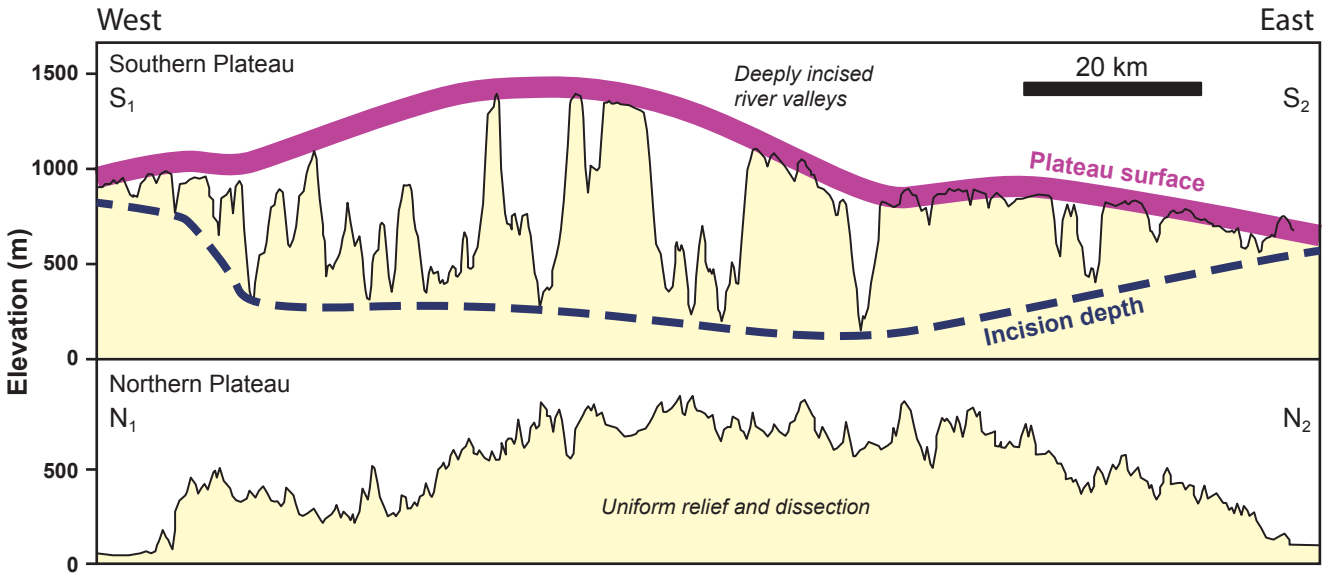
West
East
Southern Plateau
S_1
S_2
Deeply incised
river valleys
20 km
Plateau surface
Incision depth
Elevation (m)
1500
1000
500
0
Northern Plateau
N_1
N_2
Uniform relief and dissection
500
0

Fig. 5

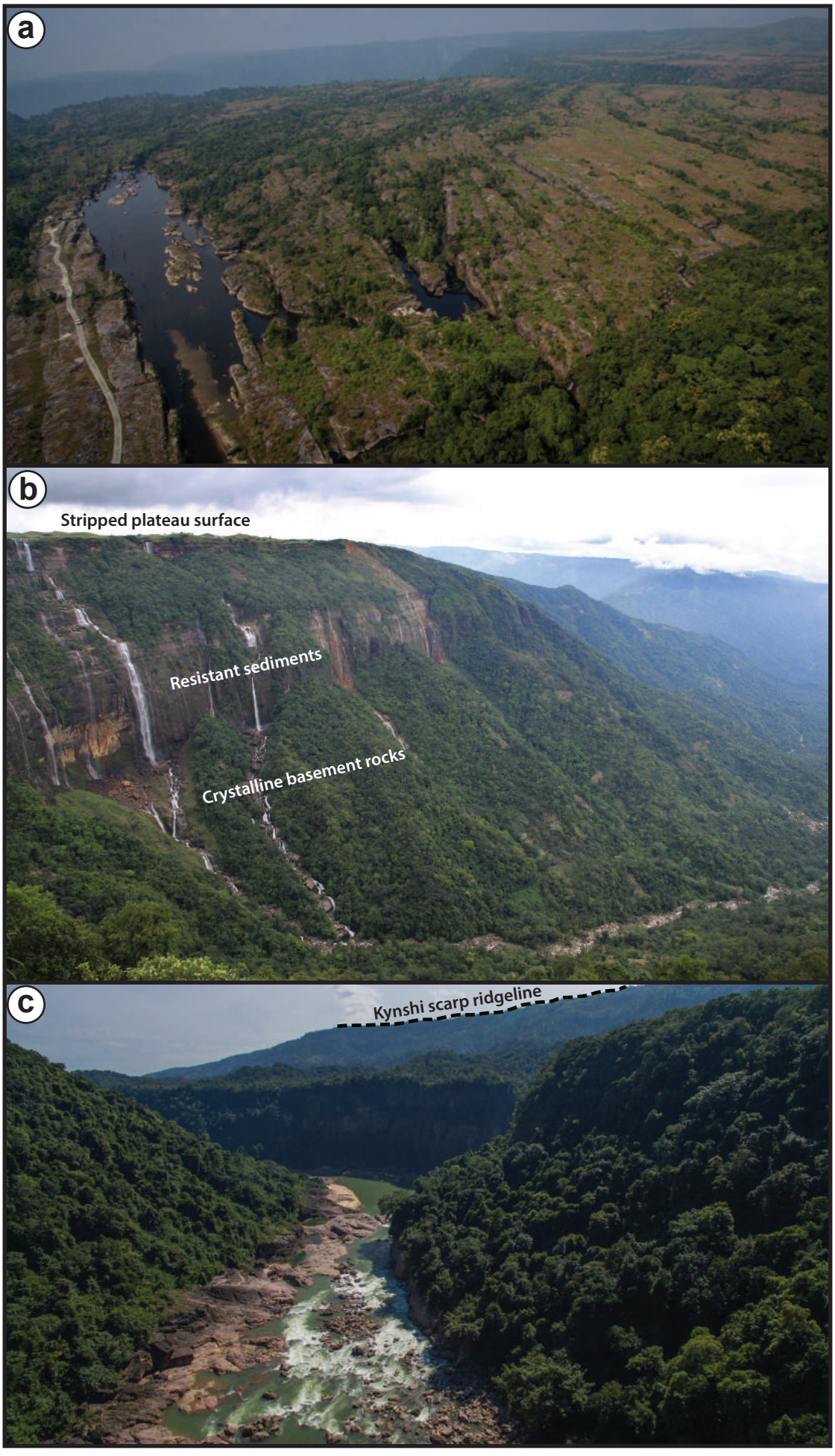
a
b
Stripped plateau surface
Resistant sediments
Crystalline basement rocks
c
Kynshi scarp ridgeline

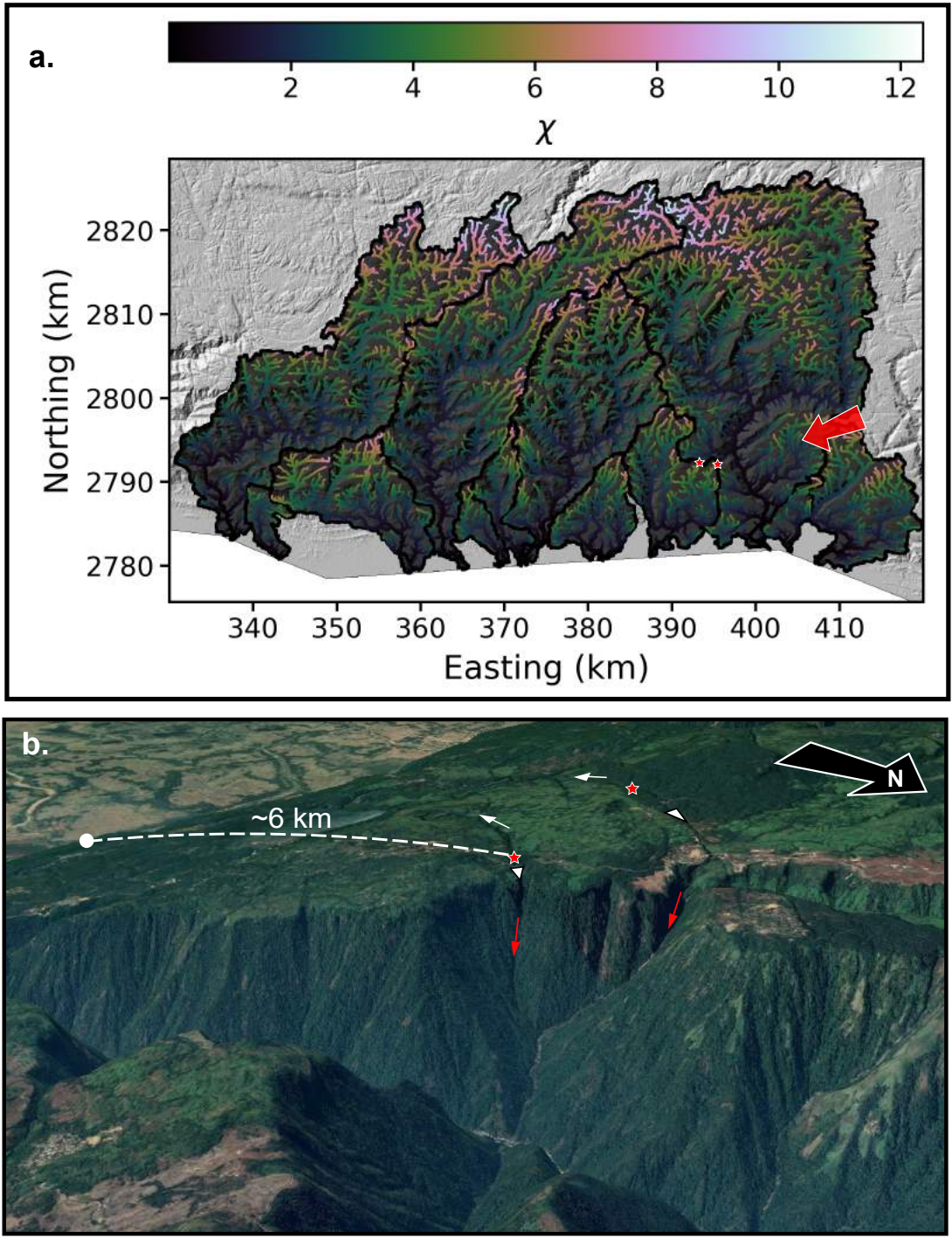
a.
2
4
6
8
10
12
χ
2820
2810
2800
2790
2780
Northing (km)
340
350
360
370
380
390
400
410
Easting (km)
b.
~6 km
N

Fig. 7

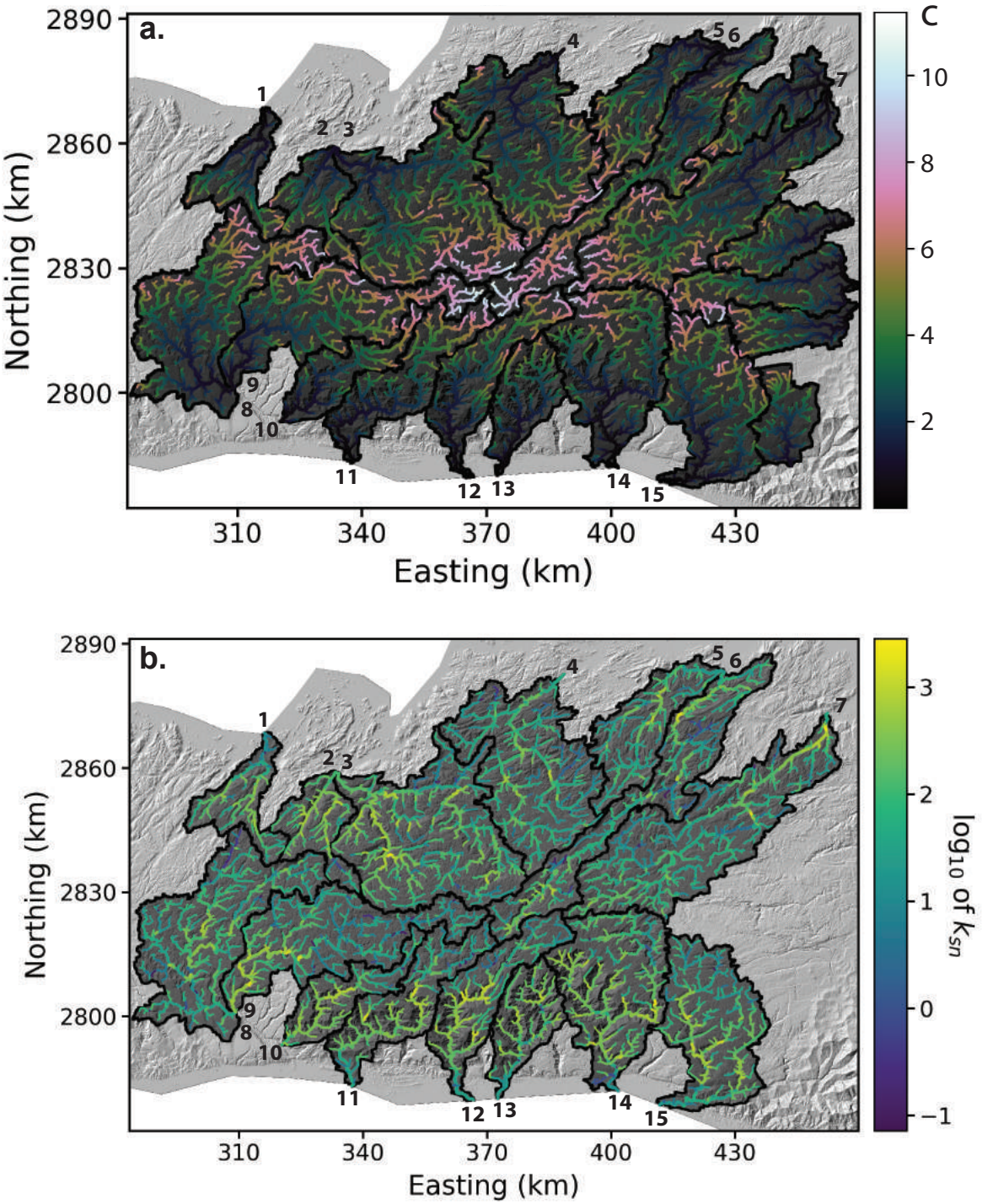
a.
b.
Northing (km)
Easting (km)
2890
2860
2830
2800
310
340
370
400
430
C
10
8
6
4
2
log10 of ksn
3
2
1
0
−1
1
2
3
4
5
6
7
8
9
10
11
12
13
14
15

Fig. 8

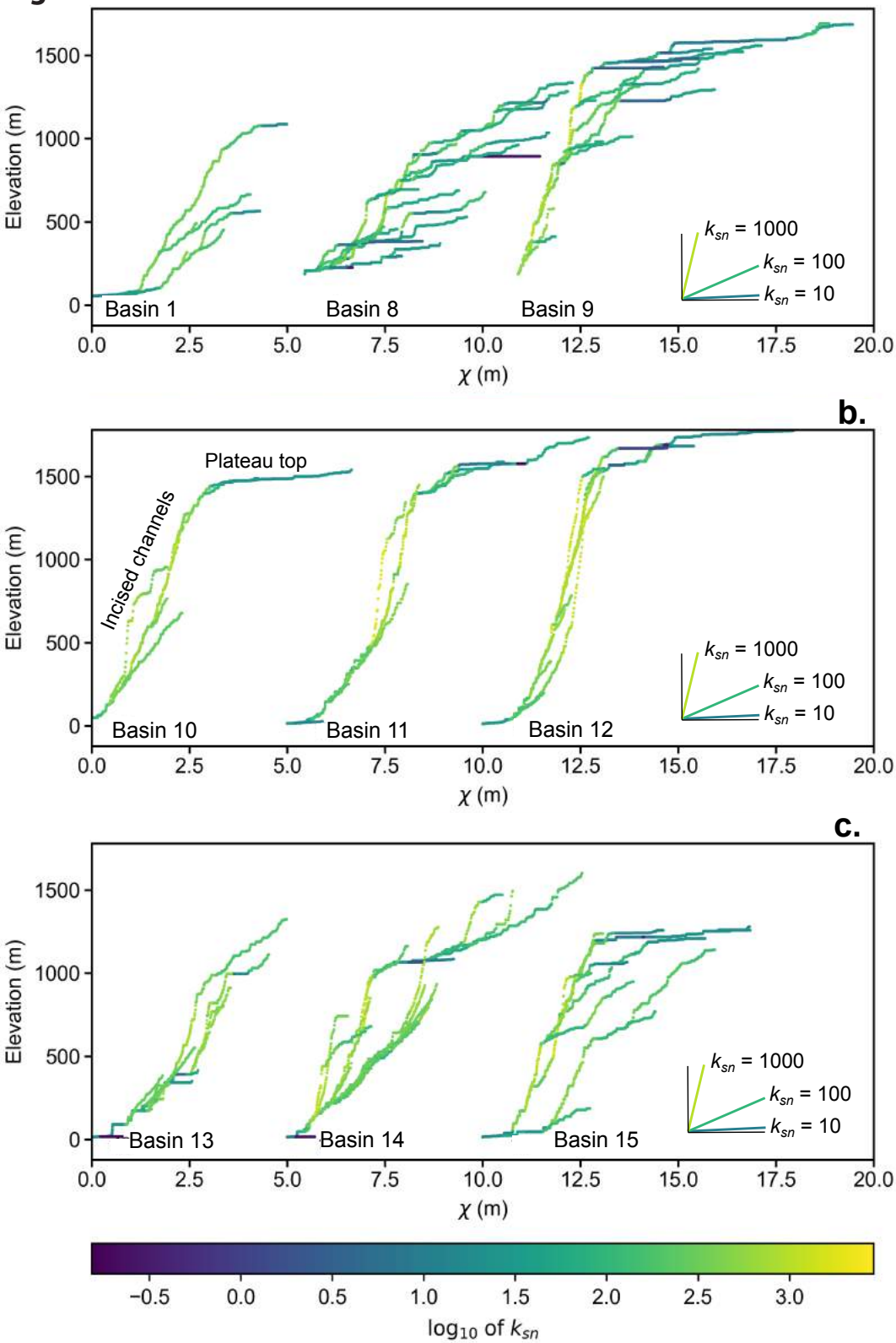
a.
Elevation (m)
1500
1000
500
0
Basin 1
Basin 8
Basin 9
k_{sn} = 1000
k_{sn} = 100
k_{sn} = 10
0.0
2.5
5.0
7.5
10.0
12.5
15.0
17.5
20.0
χ (m)
b.
Plateau top
Incised channels
Basin 10
Basin 11
Basin 12
c.
Basin 13
Basin 14
Basin 15
−0.5
0.0
0.5
1.0
1.5
2.0
2.5
3.0
$\log_{10}$ of k_{sn}

Fig. 9

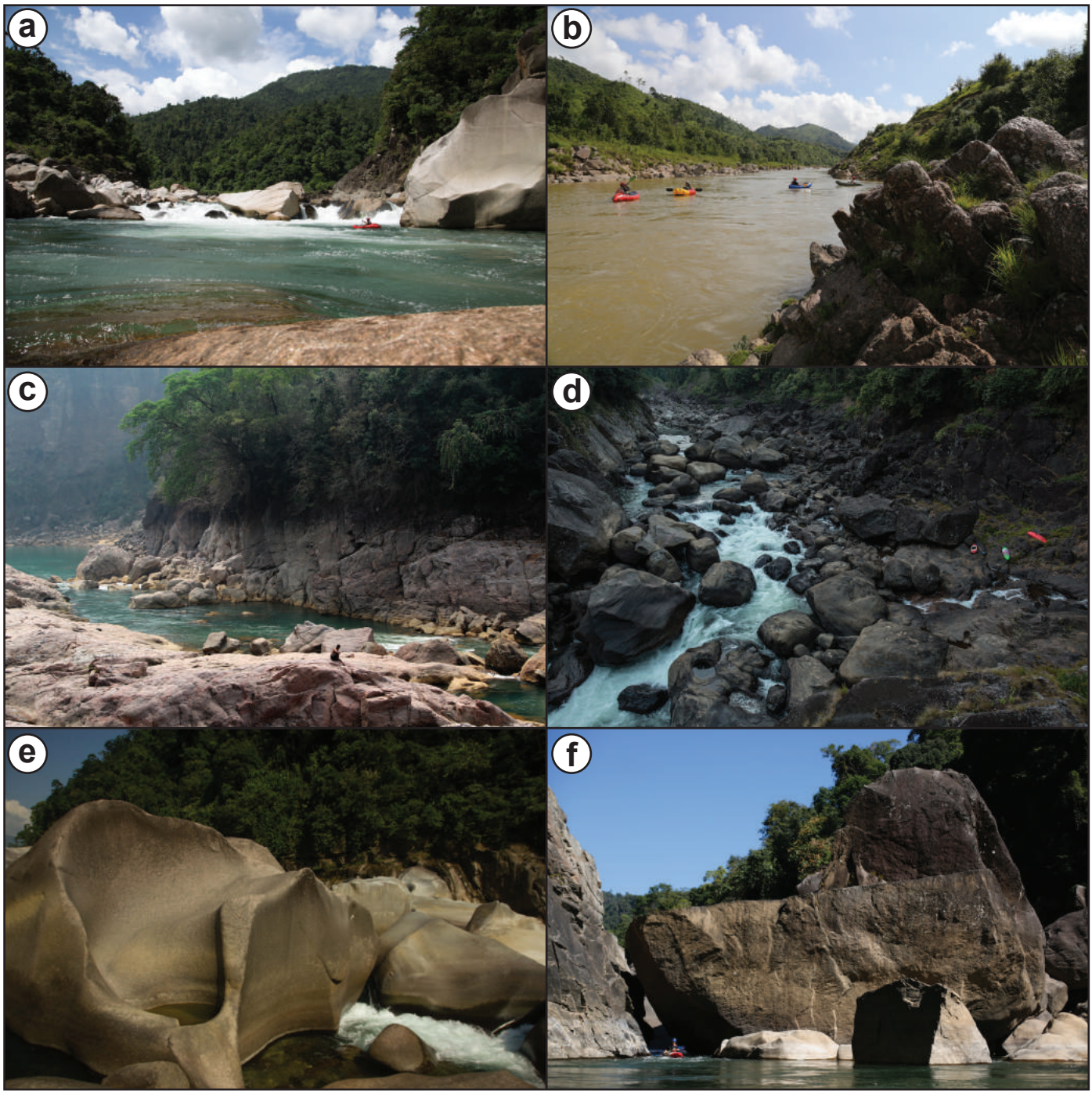

Fig. 10

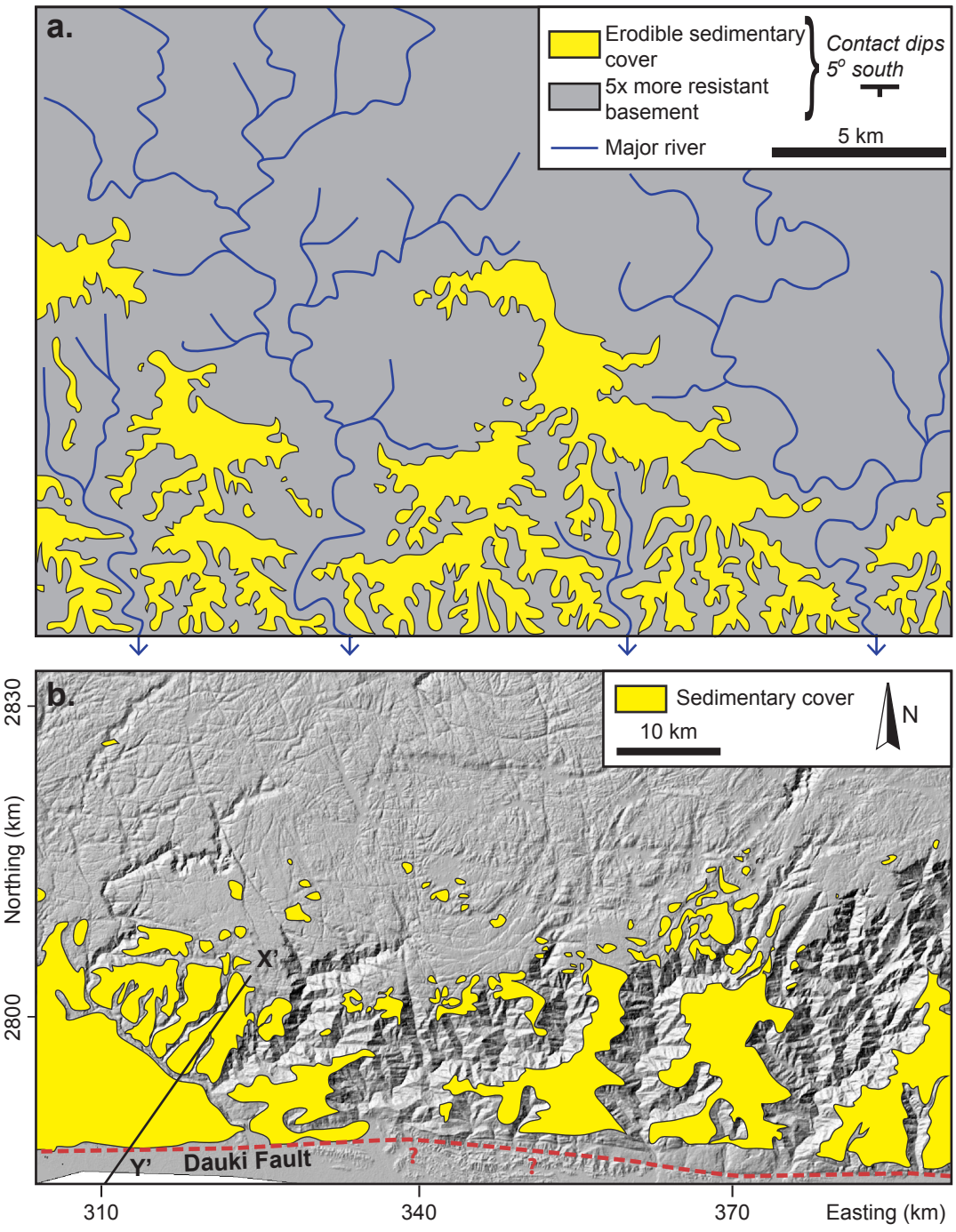
a.
Erodible sedimentary cover
5x more resistant basement
Major river
Contact dips 5° south
5 km
b.
Sedimentary cover
10 km
N
2830
2800
Northing (km)
X'
Y'
Dauki Fault
?
?
310
340
370
Easting (km)

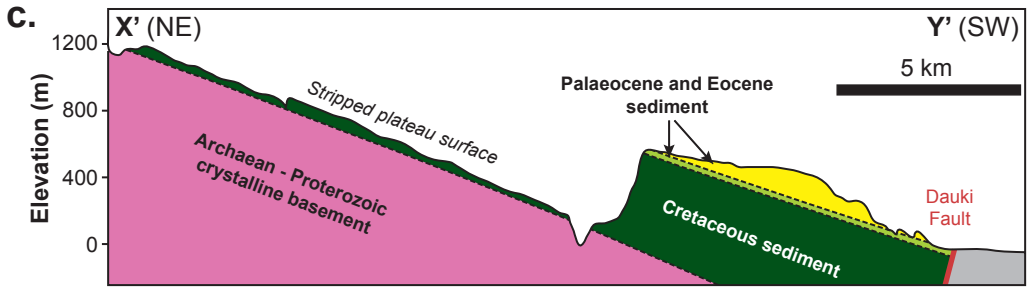
c.
X' (NE)
Y' (SW)
5 km
1200
800
400
0
Elevation (m)
Stripped plateau surface
Palaeocene and Eocene sediment
Archaean - Proterozoic crystalline basement
Cretaceous sediment
Dauki Fault

Fig. 11

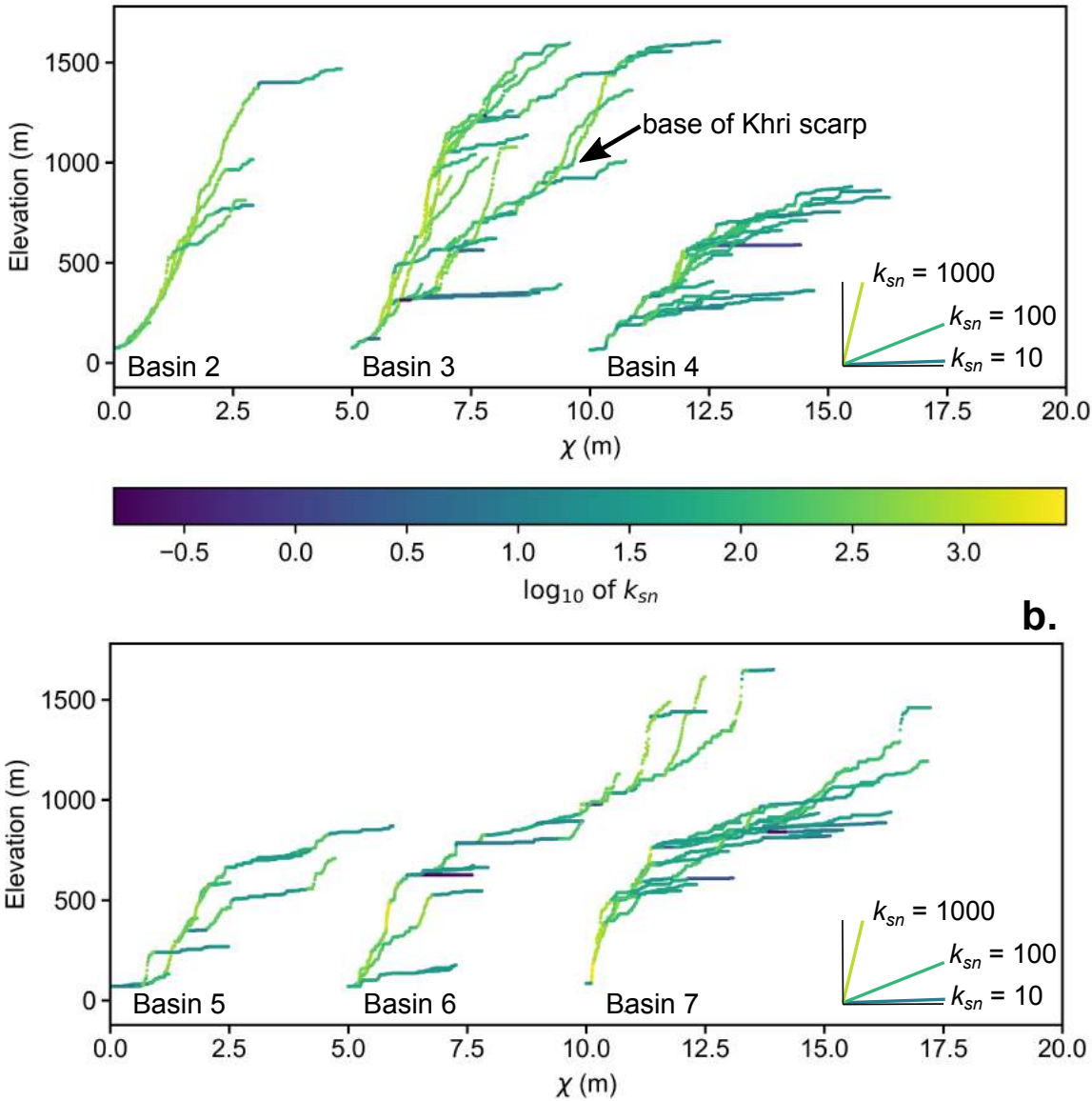
a.
Elevation (m)
1500
1000
500
0
base of Khri scarp
k_{sn} = 1000
k_{sn} = 100
k_{sn} = 10
Basin 2
Basin 3
Basin 4
0.0
2.5
5.0
7.5
10.0
12.5
15.0
17.5
20.0
χ (m)
−0.5
0.0
0.5
1.0
1.5
2.0
2.5
3.0
log10 of k_{sn}
b.
Elevation (m)
1500
1000
500
0
k_{sn} = 1000
k_{sn} = 100
k_{sn} = 10
Basin 5
Basin 6
Basin 7
0.0
2.5
5.0
7.5
10.0
12.5
15.0
17.5
20.0
χ (m)

Fig. 12

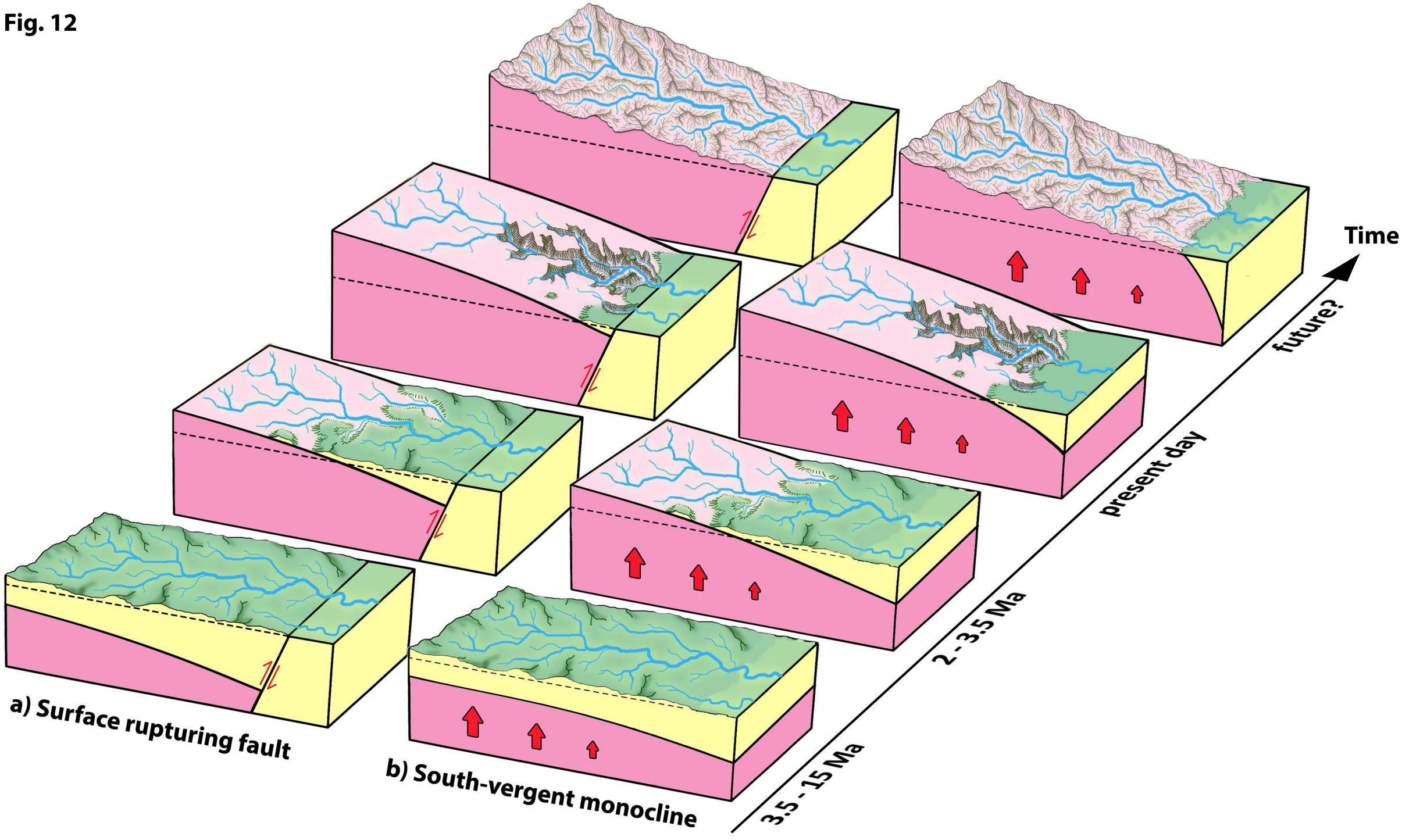
Time
future?
present day
2 - 3.5 Ma
3.5 - 15 Ma
a) Surface rupturing fault
b) South-vergent monocline

Fig. 1 (Greyscale)

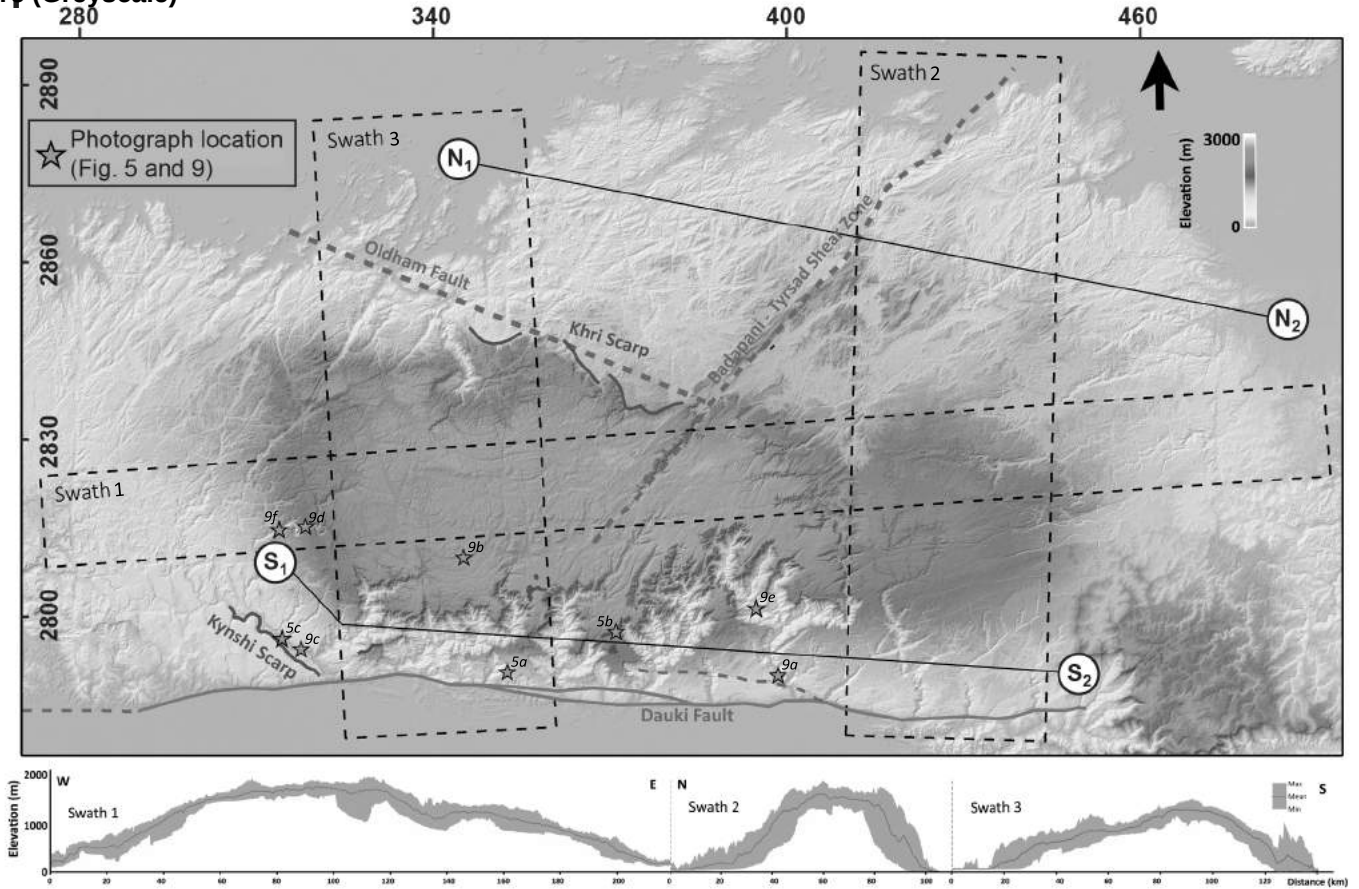

Fig. 2

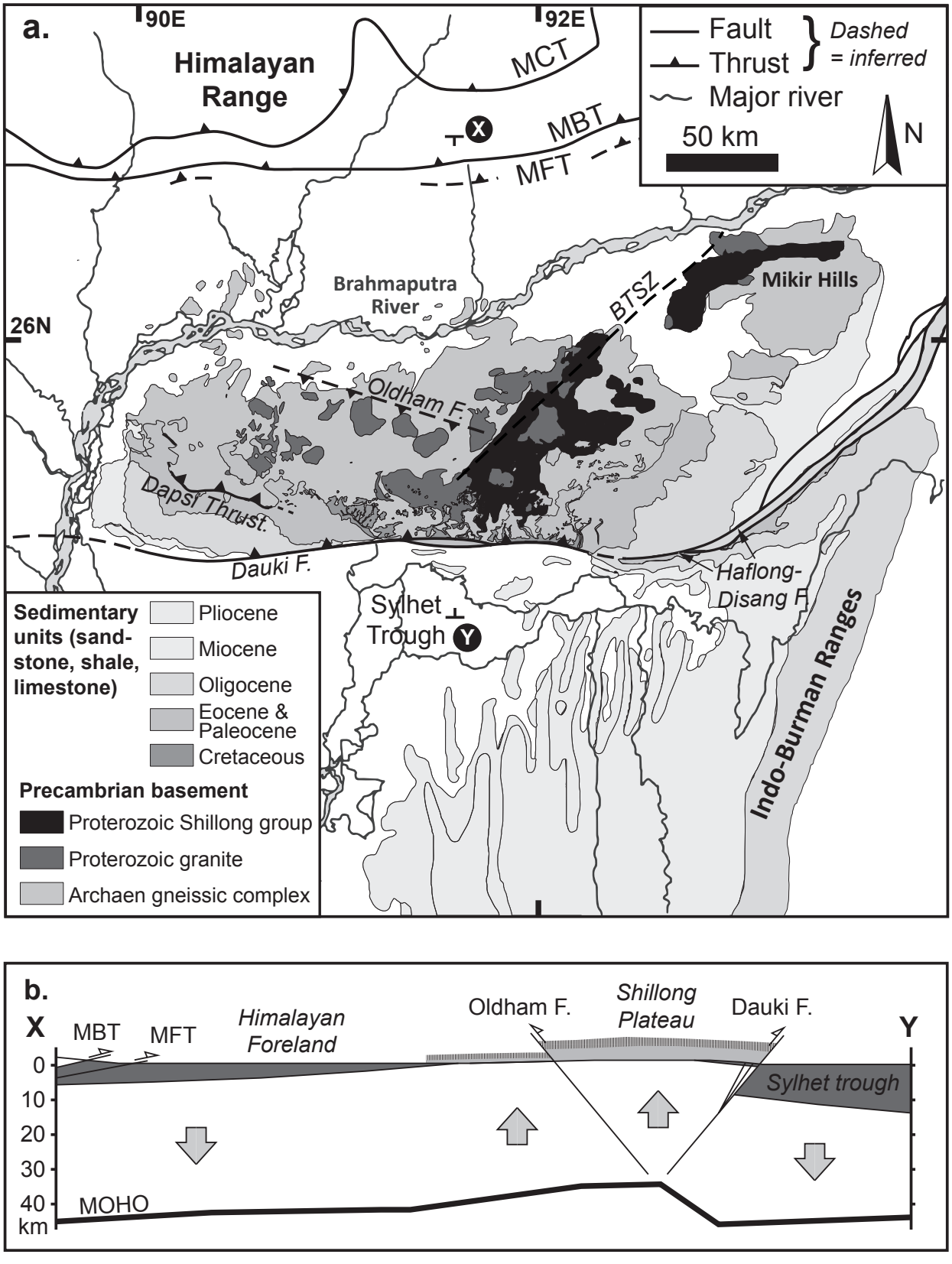
a.
90E
92E
Himalayan Range
MCT
MBT
MFT
X
Fault
Thrust
Major river
Dashed = inferred
50 km
N
Brahmaputra River
BTSZ
Mikir Hills
26N
Oldham F.
Dapsi Thrust
Dauki F.
Haflong-Disang F.
Sylhet Trough
Y
Indo-Burman Ranges
Sedimentary units (sand-stone, shale, limestone)
Pliocene
Miocene
Oligocene
Eocene & Paleocene
Cretaceous
Precambrian basement
Proterozoic Shillong group
Proterozoic granite
Archaen gneissic complex
b.
X
MBT
MFT
Himalayan Foreland
Oldham F.
Shillong Plateau
Dauki F.
Y
Sylhet trough
0
10
20
30
40
km
MOHO

Fig. 3

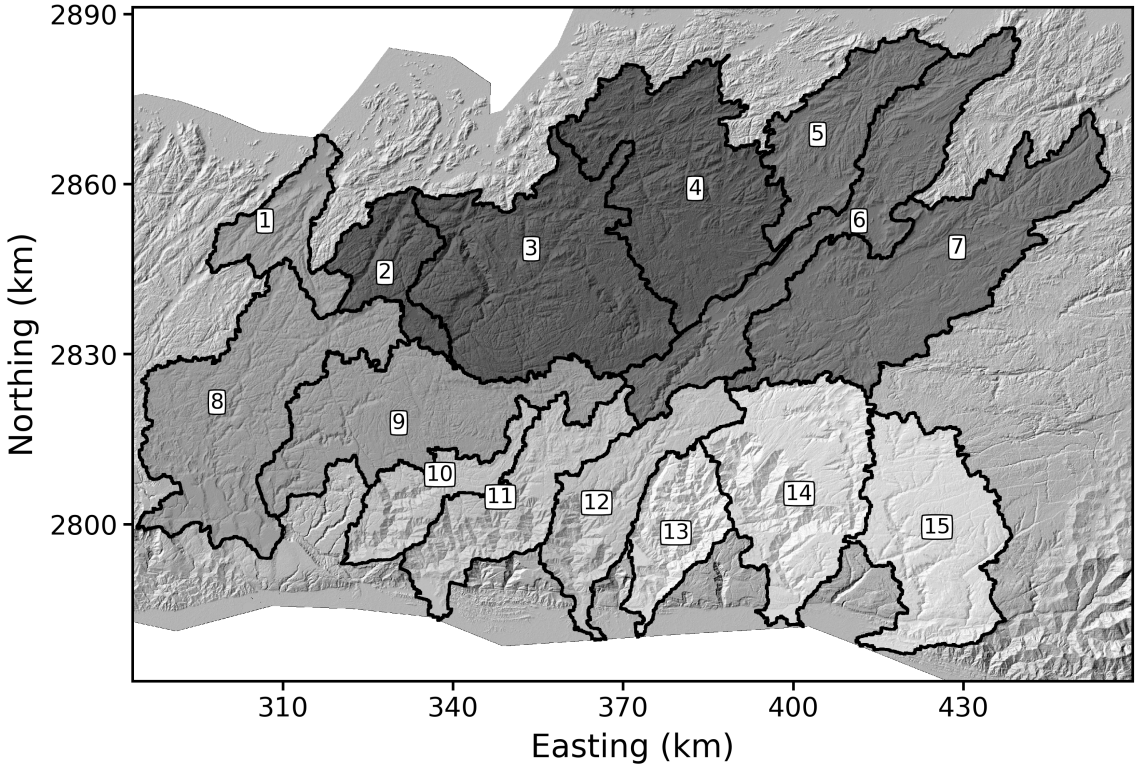
2890
2860
2830
2800
Northing (km)
310
340
370
400
430
Easting (km)
1
2
3
4
5
6
7
8
9
10
11
12
13
14
15

Fig. 4

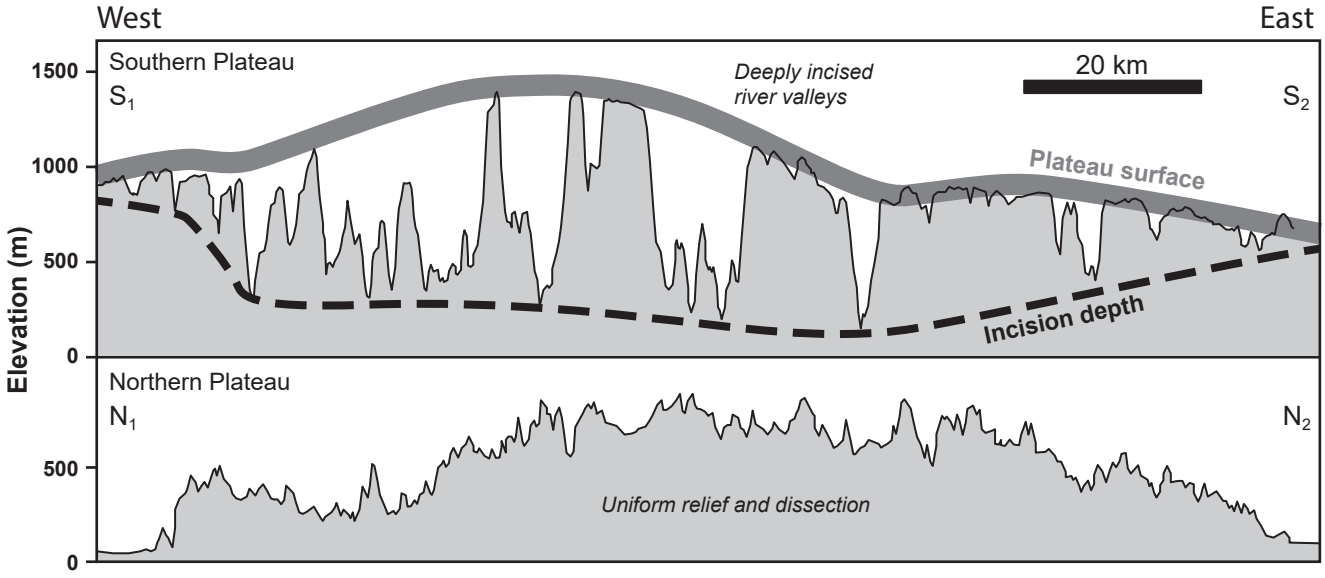
West
East
Southern Plateau
S1
Deeply incised
river valleys
20 km
S2
Plateau surface
Incision depth
Elevation (m)
1500
1000
500
0
Northern Plateau
N1
N2
Uniform relief and dissection
500
0

Fig. 5

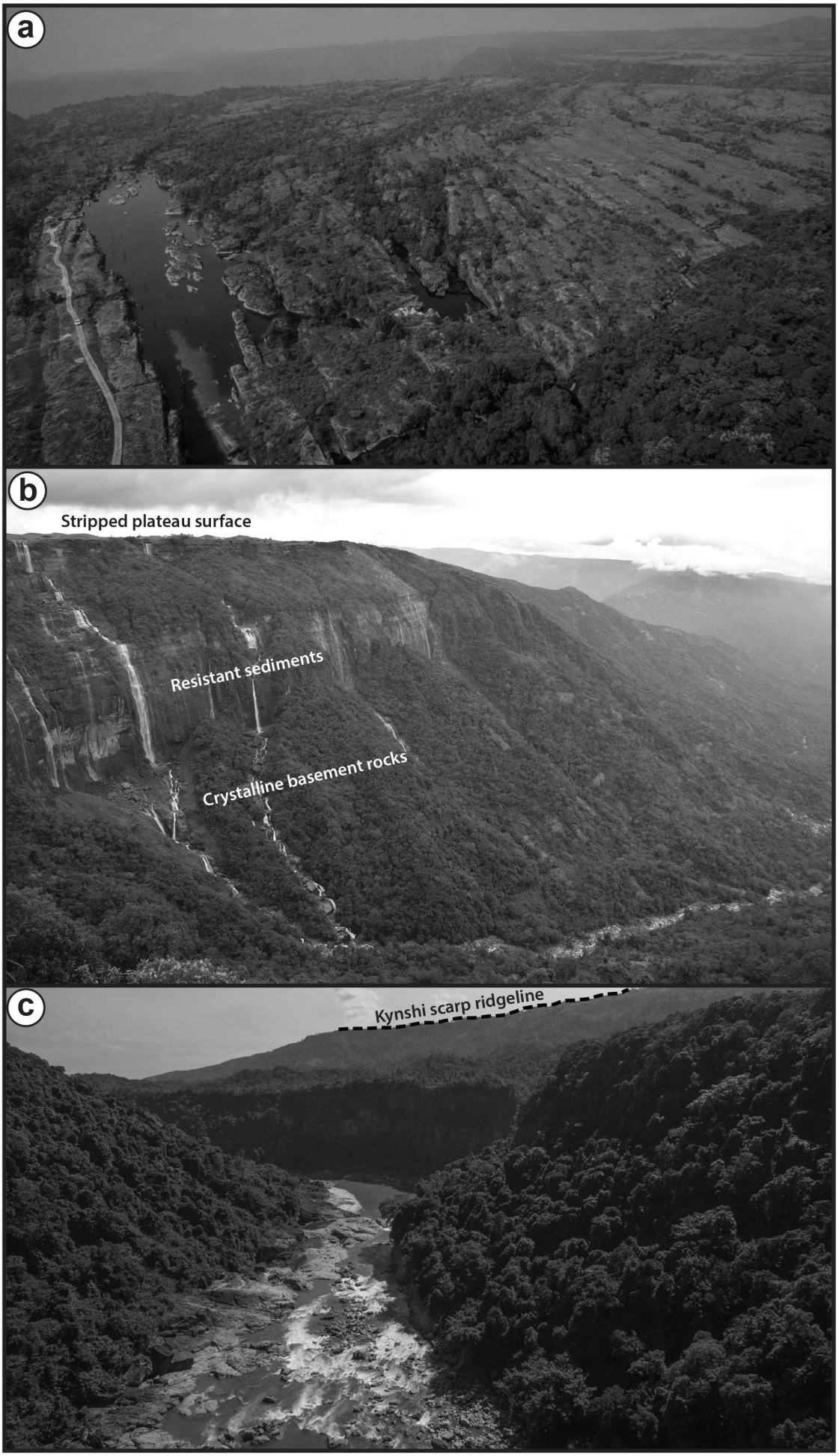
a
b
Stripped plateau surface
Resistant sediments
Crystalline basement rocks
c
Kynshi scarp ridgeline

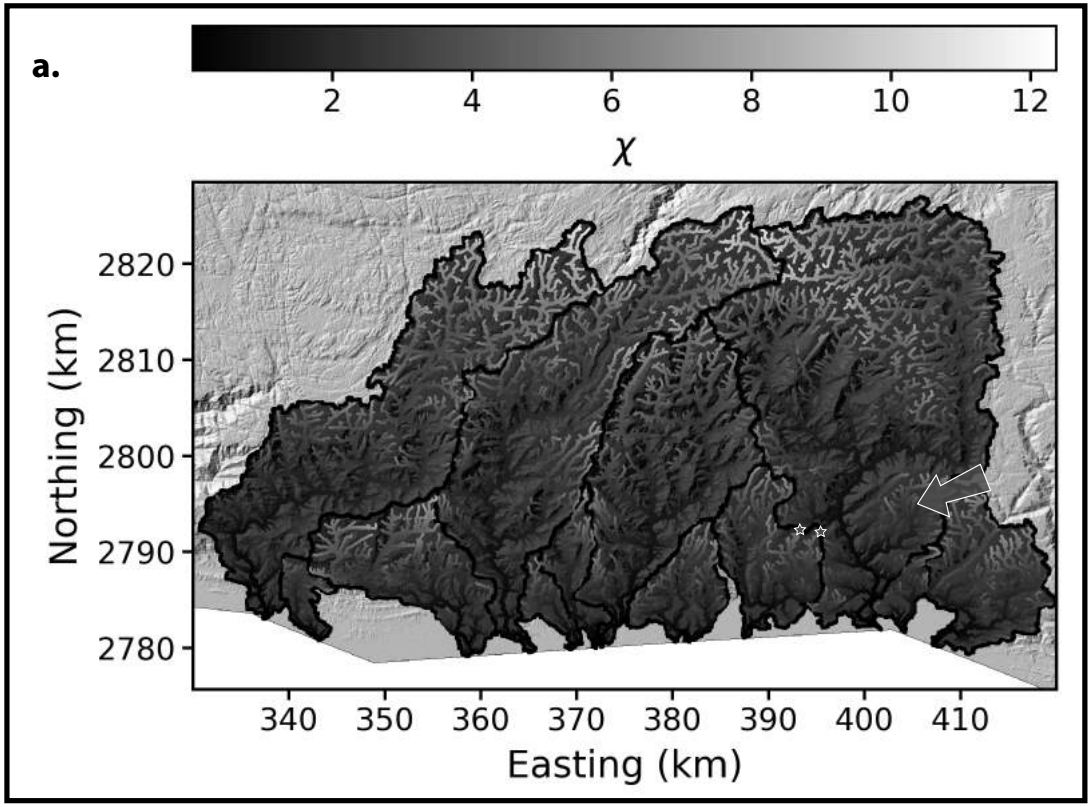
a.
2
4
6
8
10
12
χ
2820
2810
2800
2790
2780
Northing (km)
340
350
360
370
380
390
400
410
Easting (km)

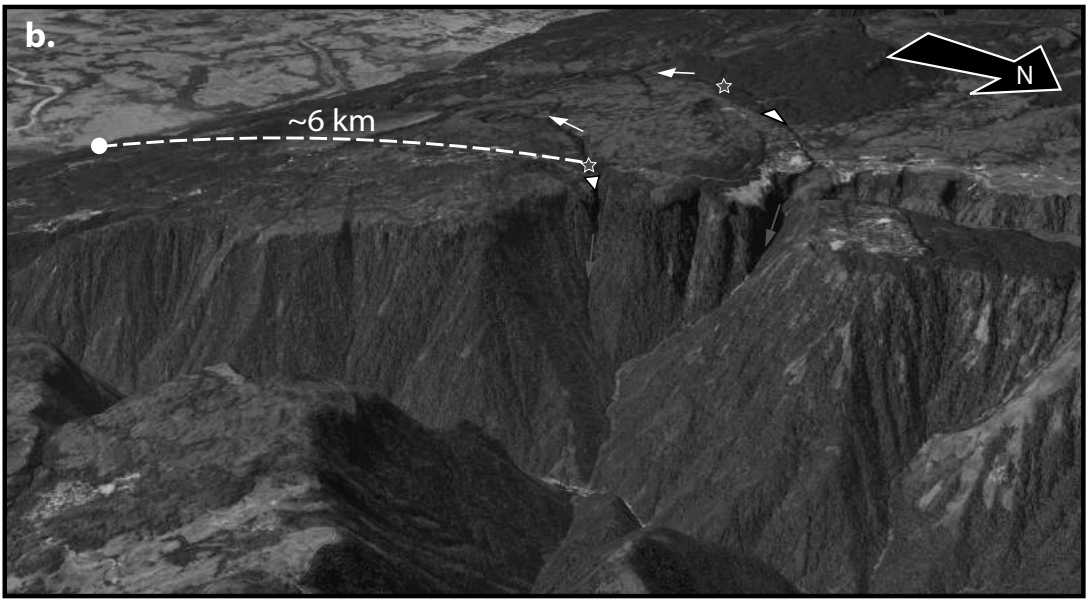
b.
~6 km
N

Fig. 7

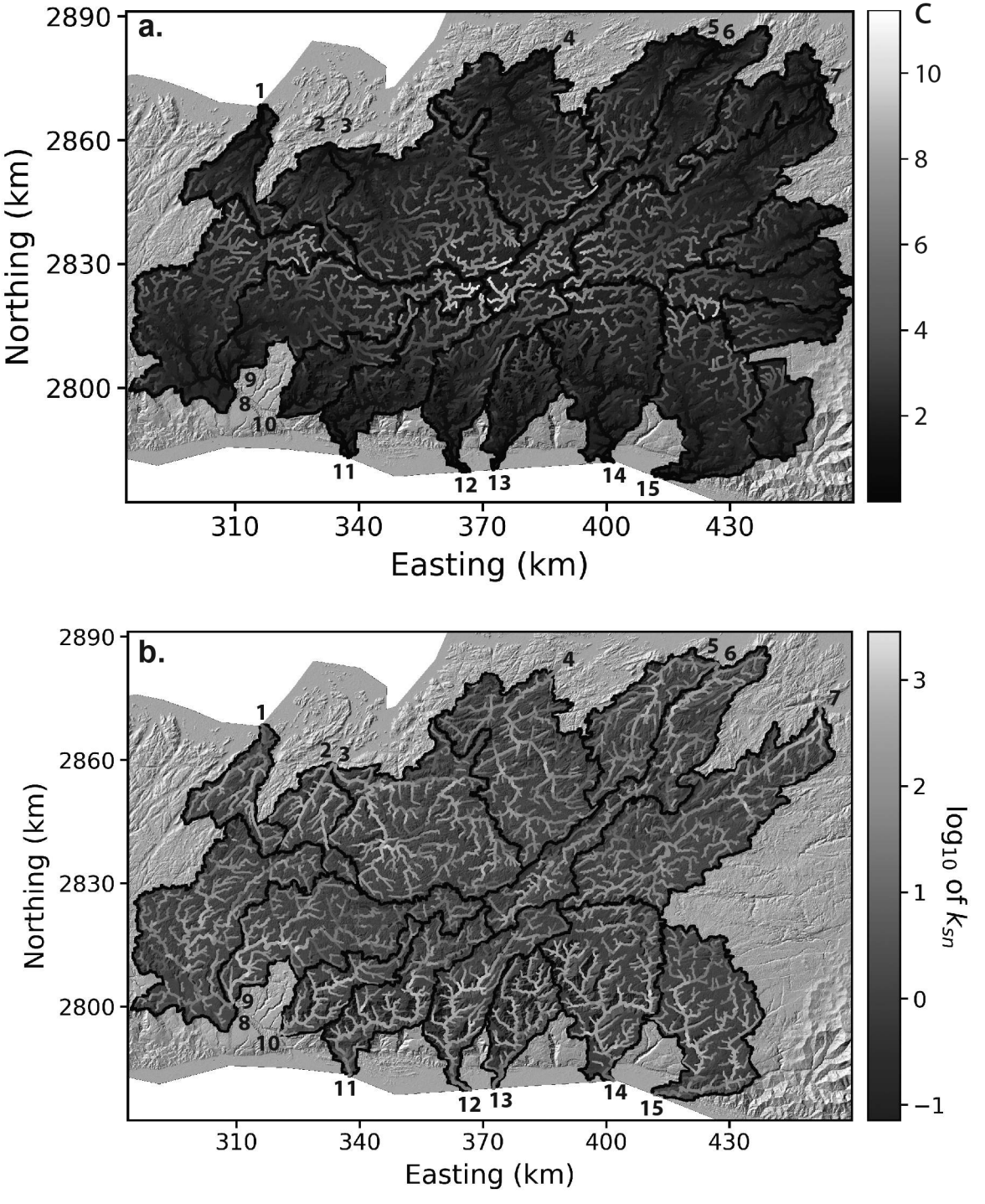
a.
b.
Northing (km)
Easting (km)
2890
2860
2830
2800
310
340
370
400
430
C
10
8
6
4
2
$\log_{10}$ of k_{sn}
3
2
1
0
−1
1
2
3
4
5
6
7
8
9
10
11
12
13
14
15

Fig. 8

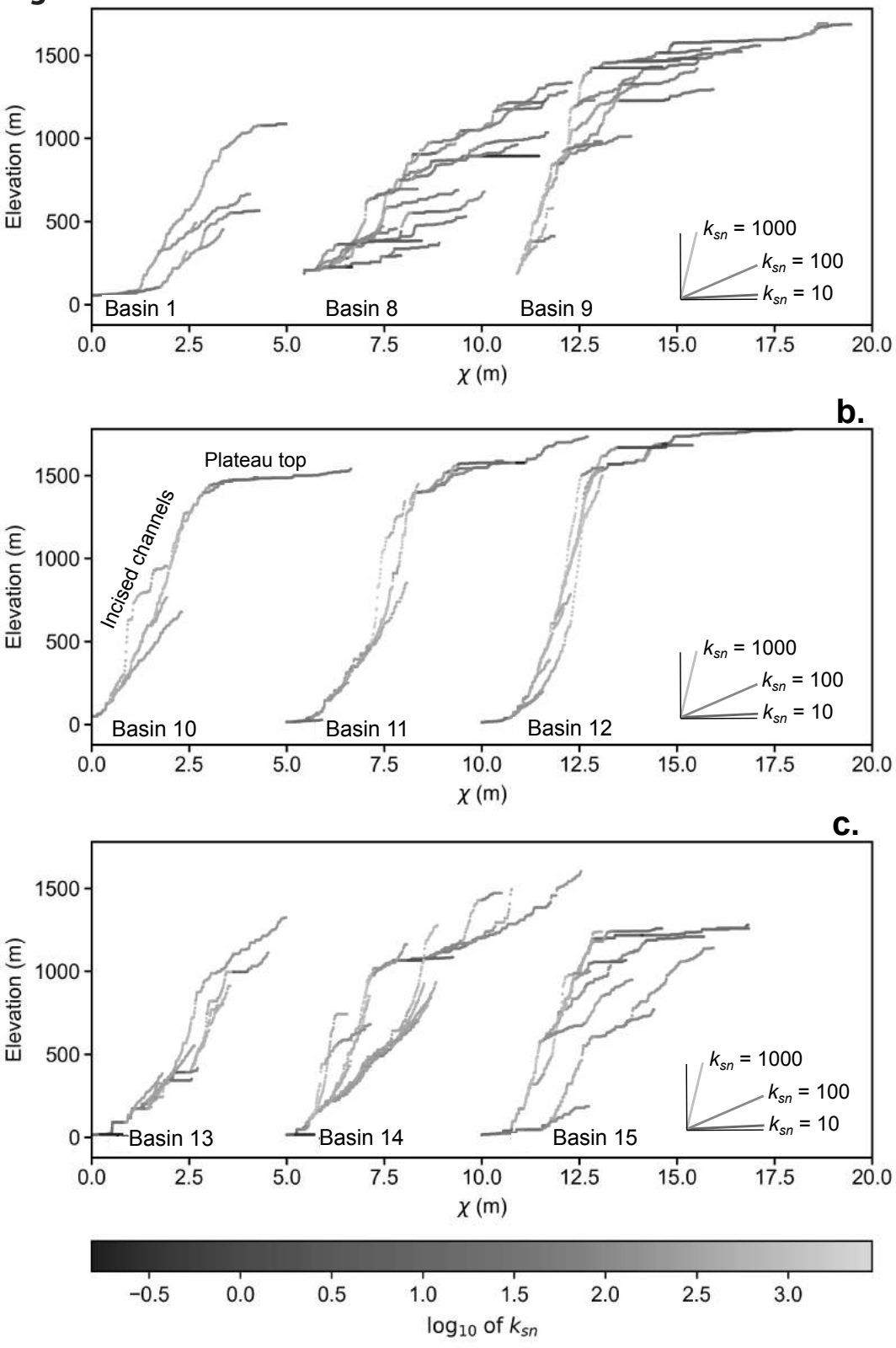
a.
Elevation (m)
1500
1000
500
0
Basin 1
Basin 8
Basin 9
k_{sn} = 1000
k_{sn} = 100
k_{sn} = 10
0.0
2.5
5.0
7.5
10.0
12.5
15.0
17.5
20.0
χ (m)
b.
Plateau top
Incised channels
Basin 10
Basin 11
Basin 12
c.
Basin 13
Basin 14
Basin 15
−0.5
0.0
0.5
1.0
1.5
2.0
2.5
3.0
$\log_{10}$ of k_{sn}

Fig. 9

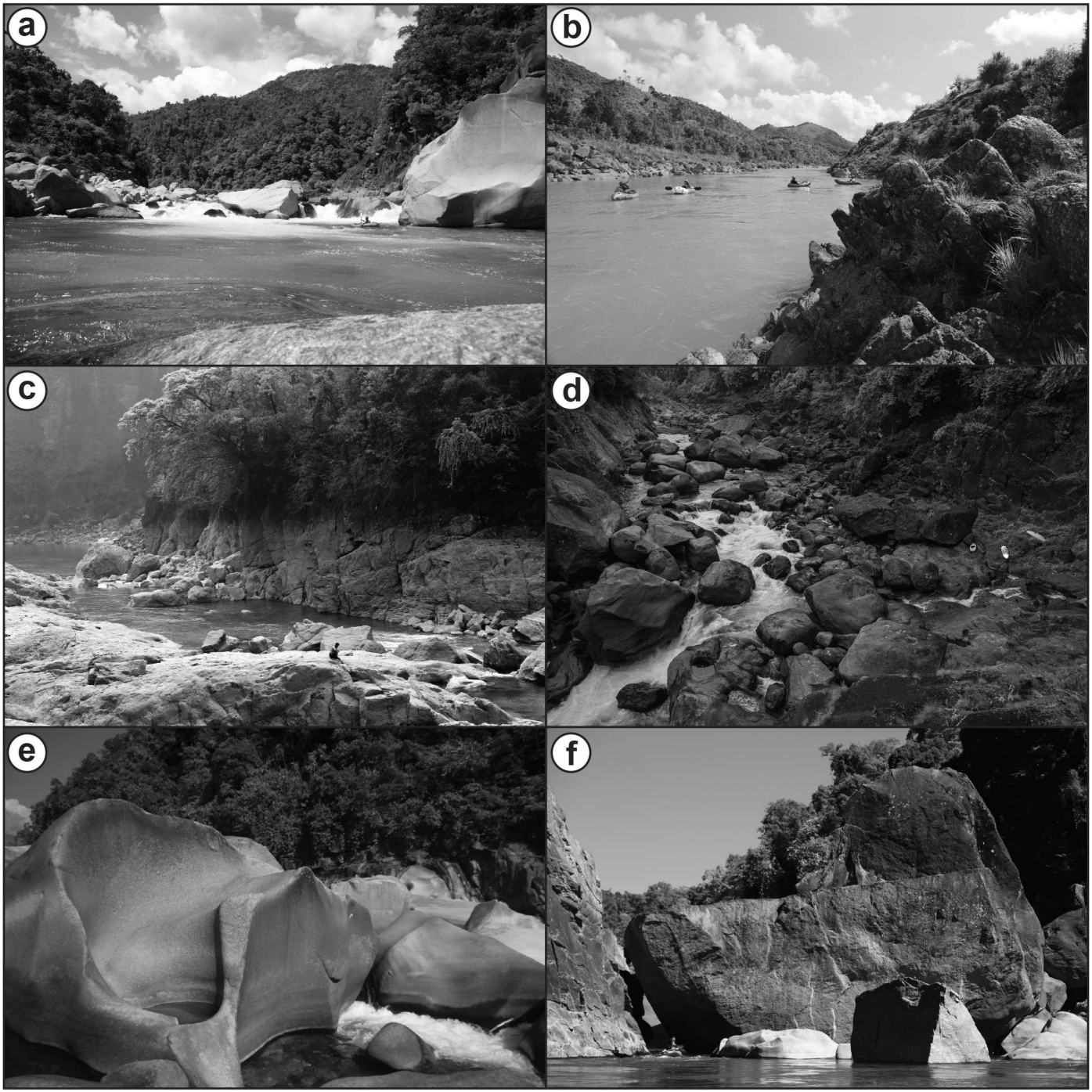

Fig. 10

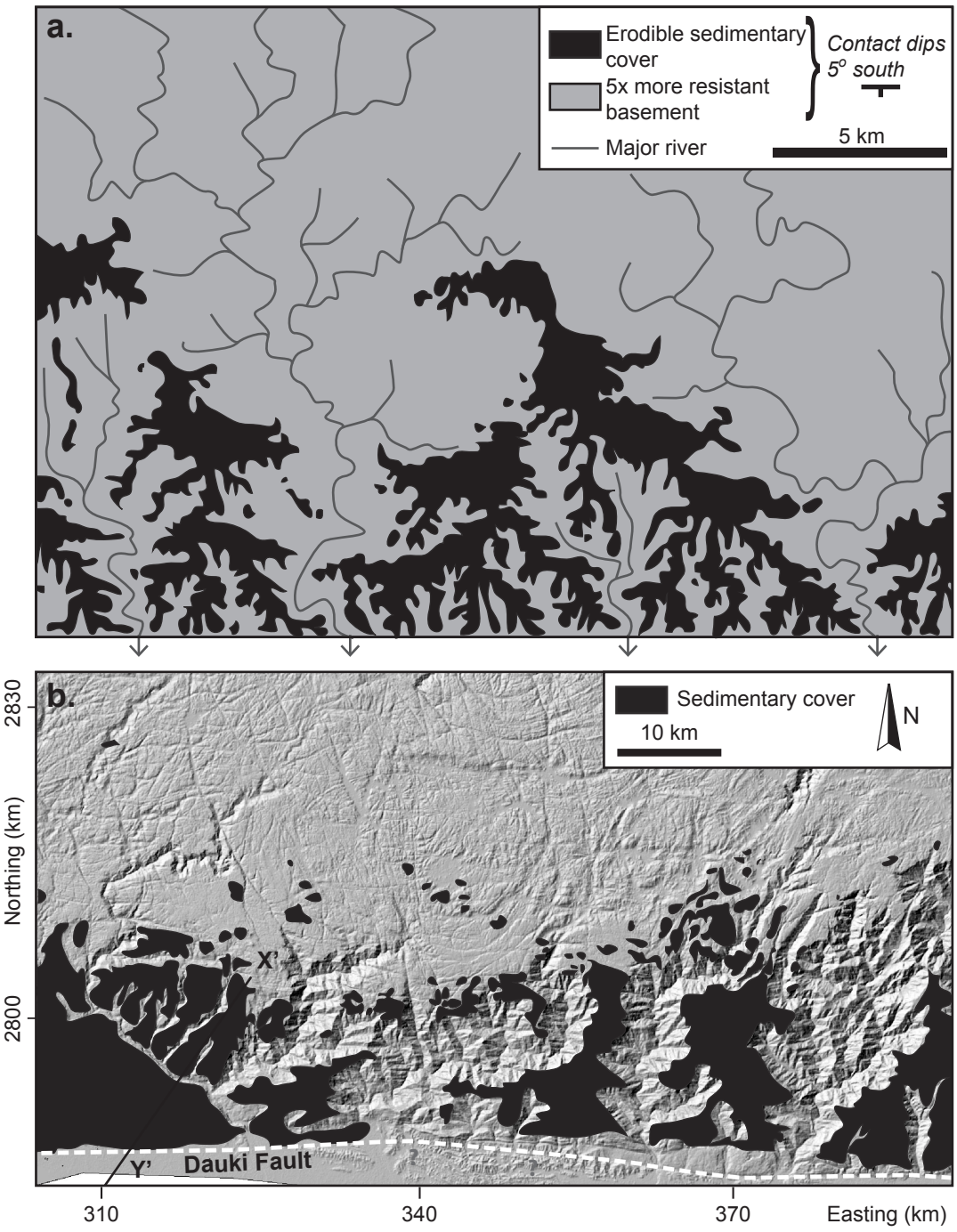
a.
Erodible sedimentary cover
5x more resistant basement
Major river
Contact dips 5° south
5 km
b.
Sedimentary cover
10 km
N
X'
Y'
Dauki Fault
2830
2800
Northing (km)
310
340
370
Easting (km)

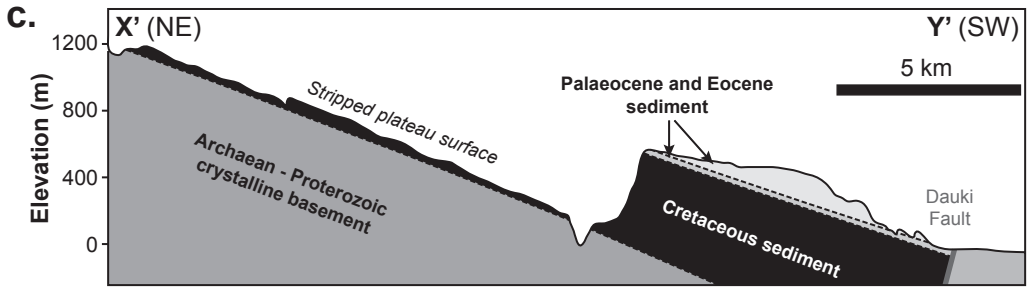
c.
X' (NE)
Y' (SW)
5 km
1200
800
400
0
Elevation (m)
Stripped plateau surface
Palaeocene and Eocene sediment
Archaean - Proterozoic crystalline basement
Cretaceous sediment
Dauki Fault

Fig. 11

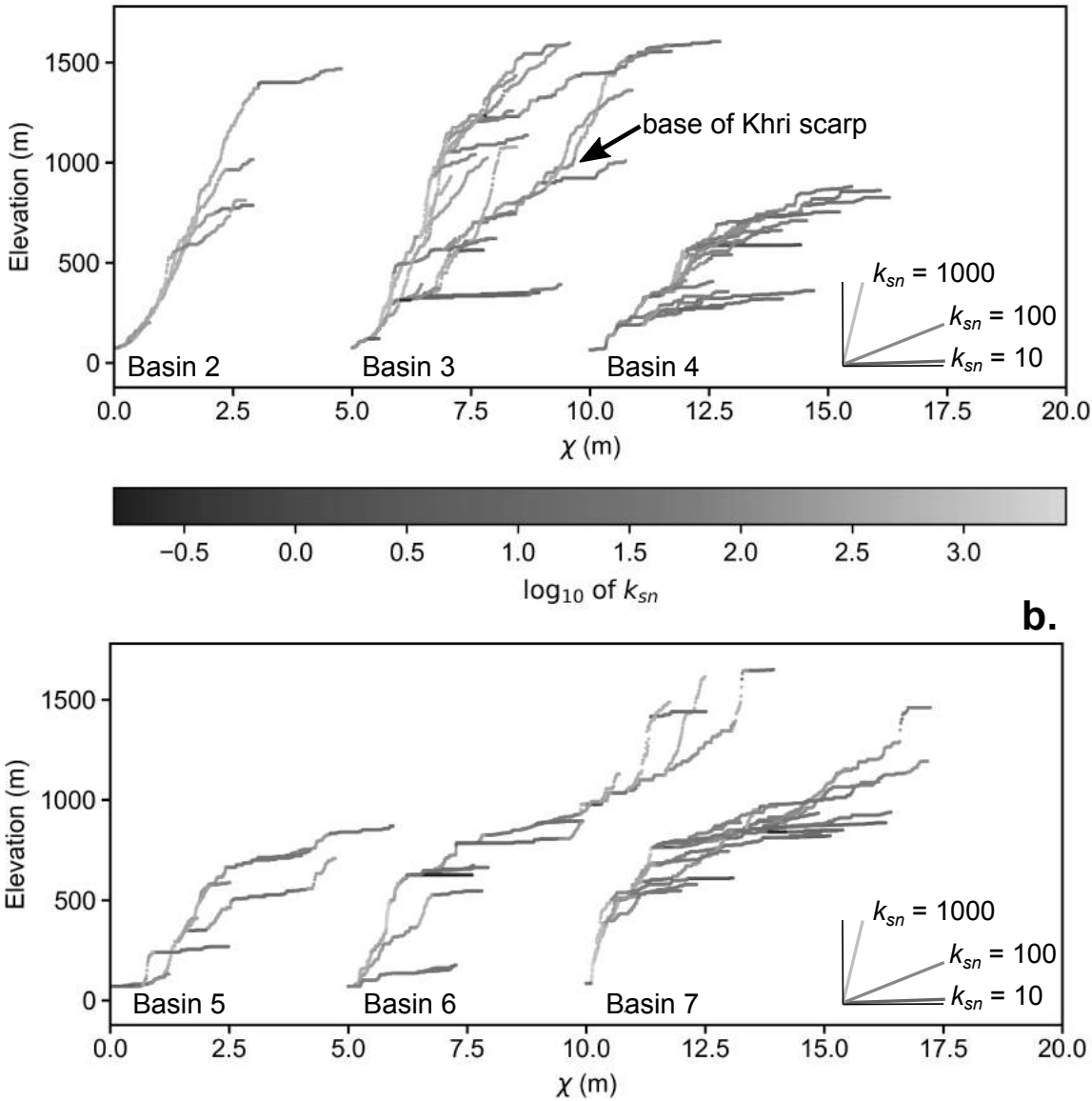
a.
Elevation (m)
1500
1000
500
0
base of Khri scarp
k_{sn} = 1000
k_{sn} = 100
k_{sn} = 10
Basin 2
Basin 3
Basin 4
0.0
2.5
5.0
7.5
10.0
12.5
15.0
17.5
20.0
χ (m)
−0.5
0.0
0.5
1.0
1.5
2.0
2.5
3.0
$\log_{10}$ of k_{sn}
b.
Elevation (m)
1500
1000
500
0
k_{sn} = 1000
k_{sn} = 100
k_{sn} = 10
Basin 5
Basin 6
Basin 7
0.0
2.5
5.0
7.5
10.0
12.5
15.0
17.5
20.0
χ (m)

Fig. 12

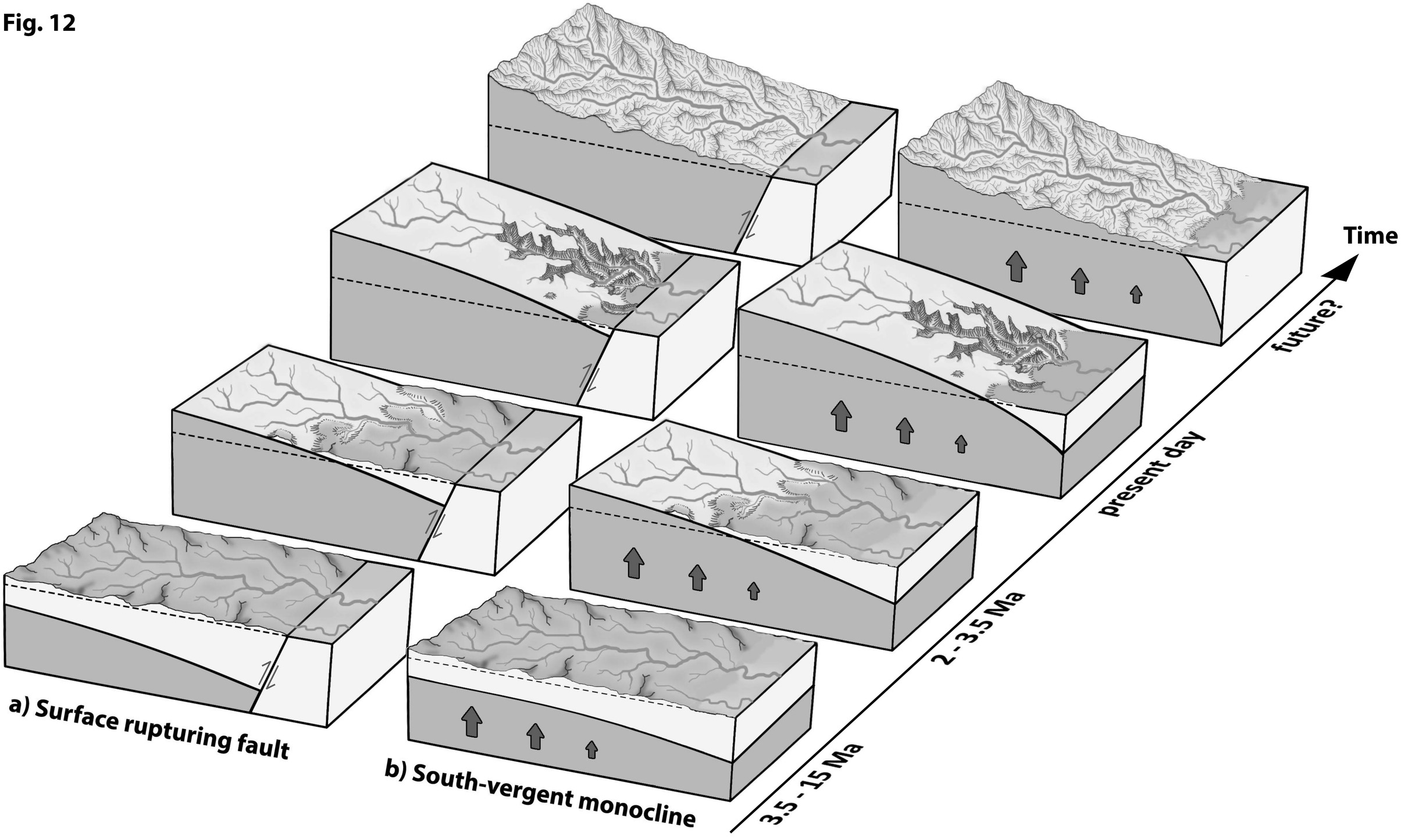
Time
future?
present day
2 - 3.5 Ma
3.5 - 15 Ma
a) Surface rupturing fault
b) South-vergent monocline